Lifetimes of ^{32}S levels

A. Kangasmäki, P. Tikkanen, and J. Keinonen
Accelerator Laboratory, P.O. Box 43, FIN-00014 University of Helsinki, Finland

W. E. Ormand
Department of Physics and Astronomy, Louisiana State University, Baton Rouge, Louisiana 70803-4001

S. Raman
Physics Division, Oak Ridge National Laboratory, Oak Ridge, Tennessee 37831

Zs. Fülöp, Á. Z. Kiss, and E. Somorjai
Institute of Nuclear Research of the Hungarian Academy of Sciences, P.O. Box 51, H-4001 Debrecen, Hungary
(Received 14 January 1998)

Mean lifetimes of 20 out of 31 bound levels in ^{32}S below an excitation energy of 8.0 MeV are deduced from the Doppler-broadened γ-ray line shapes produced in the reactions ^{2}H(^{31}P,$n\gamma$)^{32}S, ^{28}Si(^{6}Li,$pn\gamma$)^{32}S, and ^{31}P(p,γ)^{32}S. Of the 20 levels, lifetimes for 4 are reported here for the first time. For the remaining 16 levels, the lifetime values obtained in this work are considered to be more reliable and accurate than those reported in the literature. Compared to lifetime measurements reported in the literature, significant procedural improvements have been made by (i) using the entire line shape in the data analysis, (ii) making measurements with targets implanted in high-stopping-power media, and (iii) simulating with the Monte-Carlo method the slowing-down process, experimental conditions, and the delayed feeding from higher levels to the level being analyzed. The low-lying portion of the level scheme, level lifetimes, γ-ray branchings, $E2/M1$ mixing ratios, and reduced transition probabilities are compared with shell-model calculations. The reduced $B(E2)$ values for 16 out of 18 transitions and $B(M1)$ values for 5 out of 10 transitions are reproduced to within a factor of 5. A one-to-one correspondence between 33 experimental and predicted states is established up to 8.2 MeV for both positive- and negative-parity states. [S0556-2813(98)00408-7]

PACS number(s): 21.10.Tg, 23.20.−g, 25.70.Gh, 27.30.+t

I. INTRODUCTION

The deformation of even-mass nuclei changes throughout the sd-shell [1]. In self-conjugate nuclei, this change proceeds from large prolate in $^{20}_{10}$Ne$_{10}$ and $^{24}_{12}$Mg$_{12}$ to large oblate in $^{28}_{14}$Si$_{14}$, back to large prolate in $^{32}_{16}$S$_{16}$, and again to moderately oblate in $^{36}_{18}$Ar$_{18}$ [1,2]. Both shell-model calculations [1] in the full $0d_{5/2}1s_{1/2}0d_{3/2}$ space using the W interaction of Wildenthal [3] and band-mixed Hartree-Fock calculations [4] reproduce the sign variations of the electric quadrupole moments correctly, but the predicted magnitudes show some deviations. In an earlier study of ^{24}Mg levels [5] — a nucleus with a prolate rotational band structure — it was noticed that the $E2$ reduced transition probabilities are consistently underestimated in calculations similar to those of Ref. [1]. About half of the reduced transition matrix elements differed from experimental values by more than a factor of 2. In a similar study of ^{28}Si levels [6] — a nucleus with coexisting prolate and oblate bands — about one-third of the $E2$ transition matrix elements were also found to differ by at least the same factor of 2, the values being either over- or underestimated in the calculations. It is, therefore, of interest to extend such comparisons to other self-conjugate nuclei in the *sd* shell. A natural testing ground is ^{32}S, in which spherical and prolate band structures have been suggested to coexist [7].

The ^{32}S nucleus is interesting also in other aspects. Experimentally, the excitation energies of the low-lying 0^+, 2^+, and 4^+ states suggest that this nucleus behaves like a nearly spherical vibrator. On the other hand, the experimental quadrupole moment of the first 2^+ state is negative and quite large in magnitude [8] and thus indicates a large prolate deformation. Hartree-Fock calculations yield three solutions for the 2^+ states [4] corresponding to prolate, oblate, and spherical shapes in ^{32}S, the prolate solution being lowest in energy. Nilsson-Strutinski calculations of global systematics of deformation [9] predict a primary minimum in the potential energy surface for a 4^+ state at about 4-MeV excitation energy with spherical shape and a secondary minimum at about 6-MeV excitation energy for another 4^+ state with shape parameters $\epsilon=0.63$, $\gamma=0°$ corresponding to a prolate superdeformed shape. Of these two 4^+ states, the lower one is identified with the experimental 4.459-MeV level belonging to the ground-state band, while the higher one is tentatively identified with the experimental 6.411-MeV level belonging to the first-excited $K=0$ band. Other members of this proposed superdeformed band are the bandhead 0^+ state located at 3.778 MeV and the 2^+ state at 4.282 MeV [9].

Despite the fact that ^{32}S is among the most extensively studied nuclei in the *sd* shell, essential experimental data are still lacking [10,11]. Recent studies [12] at Freiburg have

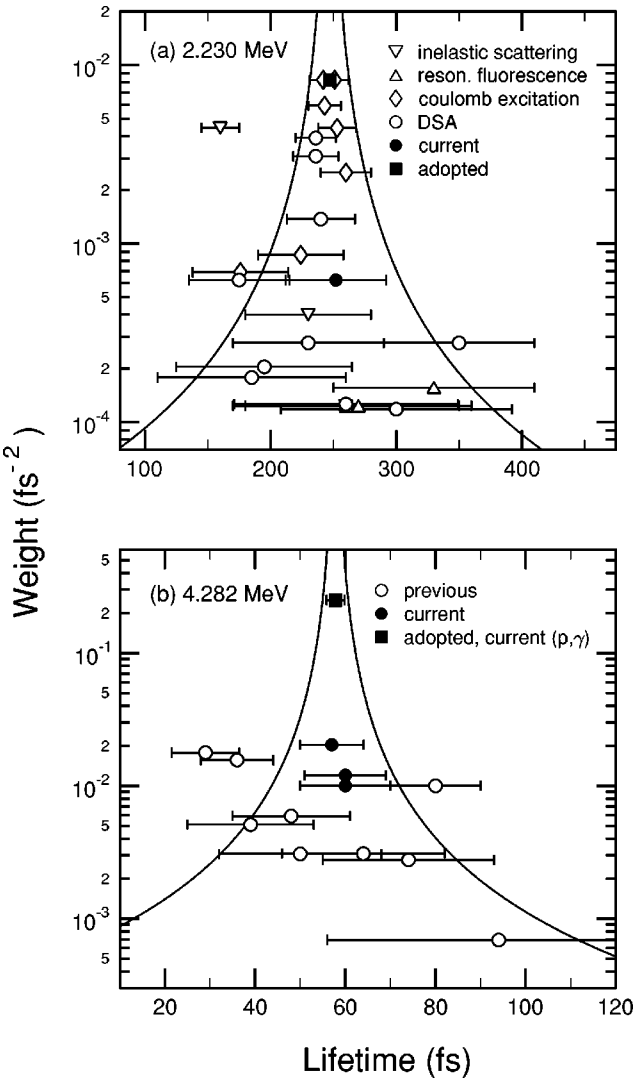

FIG. 1. A plot of the weights of lifetime measurements vs lifetime values for (a) the 2.230- and (b) 4.282-MeV levels in ^{32}S. The weight of a measurement is taken as $(\Delta\tau)^{-2}$, where $\Delta\tau$ is the quoted uncertainty. In those cases where the uncertainty of the stopping powers was not included in the quoted uncertainty, we have added quadratically 15% of the lifetime value to the statistical errors. Two contours at $\tau(\text{adopted})\pm 2(\Delta\tau)$ are also shown. For the 2.230-MeV level the adopted value (247±11 fs) is from Raman *et al.* [35]. For the 4.282-MeV level the adopted value (57.8±2.0 fs) is from the current work, and is almost equal to the value (57.7 ±2.0 fs) from the (p,γ) measurement (see Sec. II F).

contributed considerably to our knowledge of electromagnetic observables in ^{32}S, making the spectroscopy of the $T=0$ states rather complete up to 10 MeV (for $T=1$ states up to 12 MeV). However, an important ingredient in testing model calculations — reliable lifetime data for most of the excited states in ^{32}S — is still missing. With the exception of the 2.230-MeV first-excited state, for which the lifetime values determined by several different independent methods [13–34] agree reasonably well [see Fig. 1(a)], the mean lifetimes of the remaining levels [12,14,15,27–32,34,36–50] are known only with large uncertainties [see Table I and Fig. 1(b)]. For example, in the case of the 5.006-MeV level, the reported values vary from ~250 fs to ~1550 fs.

The large variations in the lifetime values are related mainly to the difficulties encountered in applying the Doppler-shift-attenuation (DSA) method. Excluding the few inelastic electron scattering [14,15,46,49] and nuclear resonance fluorescence [47,48] studies, all lifetimes for the higher excited states have been obtained in DSA measurements [12,27–32,34,36–45,50]. A summary of the experimental conditions and analysis procedures used in different DSA experiments is presented in Table II.

The reasons behind the large variations in the previous lifetime data can be traced to the use of (i) evaporated targets with layered structures (which complicate the DSA analysis), (ii) stopping materials whose stopping powers are in most cases small and poorly known, (iii) analysis methods lacking sufficient experimental confirmation (Lindhard-Scharff-Schiøtt (LSS) stopping powers [51] in combination with Blaugrund's approximation for the large-angle scattering [61]), and (iv) reactions producing quite low recoil velocities which exacerbate problem (iii). We have obtained lifetimes for ^{32}S levels using measurement techniques and analysis procedures designed to overcome these limitations. We have used (i) implanted targets with known and stable composition and structure, (ii) slowing-down materials whose stopping powers are high and either experimentally known or deducible from existing data, (iii) realistic Monte-Carlo simulations of the slowing-down process, experimental conditions, and the delayed feeding from higher levels to the level being analyzed, and (iv) reactions that produce large recoil velocities.

The results are reported in Sec. II. The resulting lifetime data and other data from the literature on electromagnetic observables in ^{32}S are compared in Sec. III with results from untruncated *sd* shell-model calculations. A brief summary is given in Sec. IV.

II. EXPERIMENT

The reactions studied in this experiment are ^{2}H(^{31}P,$n\gamma$)^{32}S, ^{28}Si(^{6}Li,$pn\gamma$)^{32}S, and ^{31}P$(p,\gamma)^{32}$S. A preliminary report on the ^{31}P(p,γ) experiment was presented in Ref. [64]. Those results are superseded in this paper.

A. Target preparation

The deuterium targets for the ^{2}H(^{31}P,$n\gamma$) reaction were prepared by implanting ^{2}H into thick gold (high stopping power) and silicon sheets (low stopping power) with a 100-kV isotope separator in Helsinki, Finland. The low-stopping-power target backing was used to determine the initial recoil velocity distribution (for details, see Ref. [65]). The high stopping power of gold provided an effective way to measure short lifetimes. In the case of the ^{28}Si(^{6}Li,$pn\gamma$) reaction, preliminary test measurements were performed using 0.4-mm-thick single-crystal silicon sheets as targets. For the actual DSA lifetime measurements, the ^{28}Si target with high stopping power was prepared by implanting 100-keV ^{28}Si^{+} (6.2×10^{17} ions/cm^{2}) into 0.4 mm-thick tantalum sheets. The energy loss of the bombarding beam par-

TABLE I. Summary of lifetimes of levels in ^{32}S obtained in the current and previous works. Except for the inelastic electron scattering (e,e') and nuclear resonance fluorescence (γ,γ) experiments, the listed lifetime values are based on DSA measurements. The values are given as reported originally. In our notation 520 $^{300}_{100}\equiv 520^{+300}_{-100}$, 1050 *300*≡1050±300, 57.8 *20*≡57.8±2.0, etc.

E_x(keV)	τ(fs)	Reaction	Ref.[a]	E_x(keV)	τ(fs)	Reaction	Ref.[a]
3778	520 $^{300}_{100}$	^{31}P(p,γ)	[36]	5413	97 *5*	^{31}P(p,γ)	[36]
	1000 $^{300}_{200}$	^{32}S$(p,p'\gamma)$	[37]		190 *20*	^{32}S$(p,p'\gamma)$	[37]
	1050 *300*	^{32}S$(\alpha,\alpha'\gamma)$	[28]		95 *25*	^{31}P(p,γ)	[31]
	>750	^{32}S$(p,p'\gamma)$	[29]		200 *25*	^{29}Si(α,n)	[38]
	1200 *550*	^{31}P(p,γ)	[31]		160 *40*	^{31}P(p,γ)	[43]
	1460 *50*	^{29}Si(α,n)	[38]		240 *35*	See Table III	This work
	1000 *200*	^{31}P(p,γ)	[32]				
	1280 *130*	See Table III	This work	5549	60 *8*	^{31}P(p,γ)	[42]
					43 *35*	^{31}P(p,γ)	[36]
4282	29 *2*	^{31}P(p,γ)	[36]		68 *12*	^{31}P(p,γ)	[27]
	50 *13*	^{31}P(p,γ)	[27]		120 *30*	^{32}S$(p,p'\gamma)$	[29]
	74 *6*	^{32}S$(p,p'\gamma)$	[37]		100 *30*	^{31}P(p,γ)	[31]
	94 *30*	^{28}Si(α,γ)	[39]		66 *5*	^{29}Si(α,n)	[38]
	48 *13*	^{32}S$(\alpha,\alpha'\gamma)$	[28]		91 *12*	See Table III	This work
	80 *10*	^{32}S$(p,p'\gamma)$	[29]				
	36 *8*	^{31}P(p,γ)	[31]	5798	14 *2*	^{32}S(e,e')	[14]
	64 *8*	^{29}Si(α,n)	[38]		8 *5*	^{31}P(p,γ)	[31]
	39 *10*	^{32}S(n,n')	[40]		14 *7*	^{29}Si(α,n)	[44]
	57.8 *20*	See Table III	This work		<10	^{29}Si(α,n)	[38]
					9.4 *30*	See Table III	This work
4459	130 *30*	^{32}S$(\alpha,\alpha'\gamma)$	[41]				
	180 *40*	^{32}S$(\alpha,\alpha'\gamma)$	[28]	6224	60 *5*	^{31}P(p,γ)	[42]
	210 *60*	^{32}S$(p,p'\gamma)$	[29]		110 $^{50}_{30}$	^{31}P(p,γ)	[36]
	200 *90*	^{31}P(p,γ)	[32]		61 *15*	^{31}P(p,γ)	[27]
	127 *30*	^{32}S(n,n')	[40]		80 *20*	^{32}S$(p,p'\gamma)$	[29]
	207 *29*	^{4}He$(^{32}$S$,\alpha'\gamma)$	[34]		130 *40*	^{31}P(p,γ)	[30]
	207 *29*		Adopted		55 *10*	^{31}P(p,γ)	[31]
					100 *8*	^{29}Si(α,n)	[38]
4695	530 *50*	^{31}P(p,γ)	[36]		75 *15*	^{31}P(p,γ)	[43]
	170 *100*	^{31}P(p,γ)	[27]		108 *13*	See Table III	This work
	490 *90*	^{32}S$(p,p'\gamma)$	[37]				
	400 *100*	^{32}S$(p,p'\gamma)$	[29]	6411	35 *6*	^{29}Si(α,n)	[38]
	230 *55*	^{31}P(p,γ)	[31]		35 *5*	See Table III	This work
	412 *25*	^{29}Si(α,n)	[38]				
	245 *50*	^{31}P(p,γ)	[32]	6581	Not known		
	400 *40*	See Table III	This work				
				6621	370 *80*	^{31}P(p,γ)	[36]
5006	600 *100*	^{31}P(p,γ)	[42]		>1000	^{31}P(p,γ)	[27]
	1500 $^{2500}_{700}$	^{31}P(p,γ)	[36]		420 *100*	^{31}P(p,γ)	[31]
	250 *50*	^{31}P(p,γ)	[27]		1520 *210*	^{29}Si(α,n)	[38]
	750 *50*	^{32}S$(p,p'\gamma)$	[37]		560 *110*	^{31}P(p,γ)	[32]
	580 *240*	^{32}S(e,e')	[15]		810 $^{350}_{250}$	^{31}P(p,γ)	[45]
	1000 *400*	^{31}P(p,γ)	[30]		980 *250*	^{31}P(p,γ)	[43]
	350 *80*	^{31}P(p,γ)	[31]		800 *120*	See Table III	This work
	795 *55*	^{29}Si(α,n)	[38]				
	1550 *380*	^{31}P(p,γ)	[32]	6666	54 $^{13}_{9}$	^{31}P(p,γ)	[36]
	600 *140*	^{31}P(p,γ)	[43]		70 *30*	^{32}S$(p,p'\gamma)$	[29]
	700 *150*	^{32}S(n,n')	[40]		22 *7*	^{31}P(p,γ)	[31]
	380 *70*	See Table III	This work		88 *8*	See Table III	This work
				6762	>300	^{31}P(p,γ)	[45]
					280 *60*	^{29}Si$(\alpha,n\gamma)$	[12]
					375 *50*	See Table III	This work

TABLE I. (*Continued*).

E_x(keV)	τ(fs)	Reaction	Ref.[a]	E_x(keV)	τ(fs)	Reaction	Ref.[a]
6852	95 *25*	^{31}P(p,γ)	[31]	7975	<30	^{29}Si$(\alpha,n\gamma)$	[12]
7002	<5	^{31}P(p,γ)	[31]	8126	0.205 $^{130}_{100}$	^{32}S(e,e')	[46]
	2.2 *7*	See Table III	This work		0.150 *30*	^{32}S(γ,γ)	[47]
					0.220 *35*	^{32}S(γ,γ)	[48]
7115	<5	^{31}P(p,γ)	[31]		0.240 *40*	^{32}S(e,e')	[49]
	2.5 *5*	See Table III	This work		0.230 *35*		Adopted
7190	11.6 *30*	See Table III	This work	8270	<60	^{29}Si$(\alpha,n\gamma)$	[12]
7350	Not known			8346	<40	^{29}Si$(\alpha,n\gamma)$	[12]
7434	11.1 *14*	See Table III	This work	9024[c]	265 *55*	^{29}Si$(\alpha,n\gamma)$	[12]
7485	7.1 *17*	See Table III	This work	9065	<20	^{28}Si(α,γ)	[50]
7536	4.7 *15*	See Table III	This work	9208	1.8 *6*	^{32}S(γ,γ)	[48]
7567[b]	150 *32*	^{29}Si$(\alpha,n\gamma)$	[12]	9235	<60	^{29}Si$(\alpha,n\gamma)$	[12]
7950	<10	^{31}P(p,γ)	[36]	9463	<70	^{29}Si$(\alpha,n\gamma)$	[12]
	110 $^{60}_{40}$	^{31}P(p,γ)	[45]				
	130 *25*	^{31}P(p,γ)	[43]	9635	90 *55*	^{29}Si$(\alpha,n\gamma)$	[12]
	210 $^{210}_{140}$	^{29}Si$(\alpha,n\gamma)$	[12]				
	210 *50*	See Table III	This work	9783	135 $^{125}_{105}$	^{29}Si$(\alpha,n\gamma)$	[12]

[a]For a particular level, the references are listed in chronological order. The actual lifetime measurements have been done at the laboratories listed below in alphabetical order: Bonn [34], Bordeaux [27], Canberra [44], Chalk River [37,29], Darmstadt [15], Freiburg [12], Giessen [47,48], Kingston [42,50], Liverpool [38], McMaster [45], MIT and NBS [49], Naval Research Laboratory [46], Oregon [36,32], Orsay [14], Oxford [28,41], Patchefstroom [31], Sofia [40], Strasbourg [39,43], and Witwatersrand [30].

[b]Up to 7.6 MeV, all known levels are listed; above only those for which there exist lifetime data.

[c]Levels above 8864 keV are proton unbound.

ticles at a target depth of 100 nm ranged from about 80 keV for 8.0-MeV ^{6}Li ions in tantalum to about 800 keV for 29-MeV ^{31}P ions in gold. A ^{31}P target with a high stopping power, essential to the measurement of short lifetimes with the ^{31}P(p,γ) reaction, was prepared by implanting 60-keV ^{31}P$^+$ (2.0×10^{17} ions/cm^2) into 0.4-mm-thick tantalum sheets. Within the implanted region of this target, the energy loss was about 5 keV for 1.5-MeV protons.

The stability of the implanted targets under beam bombardment was checked by monitoring the γ-ray yields. A further check was made by using the elastic-recoil detection analysis (ERDA) [66] and nuclear-resonance-broadening methods [67] for deducing the depth profiles of the implanted target materials both before and after the DSA measurements. The targets were quite stable with the exception that some loss of deuterium from the gold-backed target was observed in the beginning of bombardment with the ^{31}P beam. The depth distributions did not change. Based on previous studies of implanted targets [68], it was assumed that the implanted layer has no significant effect on the slowing-down of ^{32}S recoils in gold, silicon, and tantalum and, hence, on the extracted lifetimes.

Reactions ^{2}H(^{31}P,$n\gamma$)^{32}S and ^{28}Si(^{6}Li,$pn\gamma$)^{32}S

Lifetime measurements were performed at the Accelerator Laboratory of the University of Helsinki. The experimental setup used in both reactions is the same as that reported in Ref. [65]. In the case of the ^{2}H(^{31}P,$n\gamma$)^{32}S reaction, intense competition occurred from the much stronger ^{2}H(^{31}P,$p\gamma$)^{32}P reaction. In some cases the γ-ray peaks from ^{32}P were analyzed first. Lifetimes for the ^{32}P levels deduced from that analysis are reported in Ref. [65].

The ^{31}P$^{4,5+}$ and ^{6}Li^{2+} ion beams with intensities of 45–150 and 100–300 particle-nA, respectively, were supplied by the 5-MV tandem accelerator EGP-10-II at Helsinki. Bombarding energies of ~24 and ~29 MeV for ^{31}P ions and 8.0 and 12.0 MeV for ^{6}Li ions were chosen to optimize the yield and to monitor the effect of possible feeding transitions on the γ-ray line shapes. Slightly different bombarding energies of the ^{31}P beam were used (24.6 and 29.7 MeV for the gold-backed target, 24.0 and 29.0 MeV for the silicon-backed target) to ensure approximately equal center-of-mass energies for the ^{2}H(^{31}P,$n\gamma$)^{32}S reaction in both materials.

The beams were focused and collimated to a 2×2 mm^2 spot on the target that was set with its surface perpendicular

TABLE II. Summary of the experimental conditions and analysis procedures used in the lifetime measurements of ^{32}S levels using the Doppler-shift-attenuation (DSA) method.

Ref.[a]	Reaction[b] v/c (%)	(i) Slowing-down medium. (ii) Stopping powers and DSA analysis.[c]
[42]	^{31}P(p,γ) 0.27	(i) No details given. (ii) No details given.
[41]	^{32}S$(\alpha,\alpha'\gamma)$ 1.52	(i) Evaporated CdS (110 μg/cm^2) on nickel (1.2 mg/cm^2). (ii) The LSS electronic stopping power [51] was corrected by $f_e = 1.12$, extrapolated from data reported in Refs. [52–54]. See also Ref. [55]. $F(\tau)$ and Doppler-broadened line-shape analyses.
[26]	^{28}Si(α,γ) 0.54	(i) Evaporated SiO (93 μg/cm^2) on copper. (ii) The LSS electronic stopping power [51] was multiplied by a correction factor, extrapolated from data of Ormrod and co-workers [53,54,56]. The LSS nuclear stopping power [51] was approximated by an analytic expression. Uncertainty in the stopping power not included. $F(\tau)$ and Doppler-broadened line-shape analyses.
[36]	^{31}P(p,γ) 0.20	(i) Evaporated Zn_3P_2 (8–10-keV thick) on gold. (ii) $F(\tau)$ analysis.
[27]	^{31}P(p,γ) 0.20	(i) Evaporated Zn_3P_2 ($\sim$100 μg/cm^2) on gold. (ii) Uncertainty in the stopping power not included. $F(\tau)$ analysis.
[37]	^{32}S$(p,p'\gamma)$ 0.61	(i) PbS (22 mg/cm^2), MoS_2 (8 mg/cm^2), or S (5 mg/cm^2) on gold. (ii) $F(\tau)$ and Doppler-broadened line-shape analyses.
[39]	^{28}Si(α,γ) 0.63	(i) Evaporated ^{28}Si (98% ^{28}Si, 2 mg/cm^2) on copper. (ii) Uncertainty in the stopping power not included. $F(\tau)$ analysis.
[28]	^{32}S$(\alpha,\alpha'\gamma)$ 1.87	(i) Evaporated CdS (350 μg/cm^2) on gold (3 mg/cm^2). (ii) A 15% uncertainty assumed in the electronic stopping power. Slowing down in the target and backing considered. Lifetimes based on $F(\tau)$ analysis. Doppler-broadened line-shapes used only as a check.
[29]	^{32}S$(p,p'\gamma)$ 0.80	(i) S (383 μg/cm^2) on gold (100 μg/cm^2), cooled to 77 K. (ii) The effect of a 10% uncertainty in the stopping power included. Slowing down in the target and backing considered. $F(\tau)$ analysis.
[30]	^{31}P(p,γ) 0.14	(i) Red phosphorus compressed to a density of 2.2 g/cm^3. (ii) Stopping power uncertainty not included. $F(\tau)$ analysis.
[31]	^{31}P(p,γ) 0.20	(i) Evaporated Zn_3P_2 (10 keV thick) on Cu or Ta backing, and covered by a thin layer of Au. (ii) The electronic stopping power of the LSS theory [51] was corrected by observations of Ormrod and co-workers [54]. A 15% systematic error in the stopping power was assumed. $F(\tau)$ analysis.
[44]	^{29}Si(α,n) 1.04	(i) Evaporated SiO_2 (92% ^{29}Si, $\sim$200 μg/cm^2) on tantalum. (ii) A 15% uncertainty in the stopping power included. $F(\tau)$ analysis.
[38]	^{29}Si(α,n) 1.12	(i) $^{29}SiO_2$ (700 and 990 μg/cm^2) on gold. (ii) Slowing-down in the target and target substrate taken into account. A 25% uncertainty in the stopping power assumed but not included in the quoted lifetime values. $F(\tau)$ analysis.
[32]	^{31}P(p,γ) 0.20	(i) No details given. However, see Refs. [57,58]. (ii) A 15% uncertainty in the stopping power included. $F(\tau)$ analysis.

TABLE II. (*Continued*).

Ref.[a]	Reaction[b] v/c (%)	(i) Slowing-down medium. (ii) Stopping powers and DSA analysis.[c]
[45]	^{31}P(p,γ) 0.19	(i) Evaporated Zn_3P_2 (6-keV-thick for 1.5-MeV protons) on tantalum. (ii) A 20% uncertainty of the stopping power was included. $F(\tau)$ analysis.
[43]	^{31}P(p,γ) 0.19	(i) Evaporated P (60 and 90 μg/cm^2) on gold. (ii) The corrections by Ormrod and co-workers [54] on the LSS electronic stopping power [51] were applied. A 15% uncertainty in the stopping power was assumed and quadratically added to other errors. $F(\tau)$ analysis.
[22,24]	Mg(^{32}S,^{32}S′) 5.54	(i) Natural magnesium (78.70% ^{24}Mg; 10.13% ^{25}Mg; 11.17% ^{26}Mg; thick target).
	Si(^{32}S,^{32}S′) 5.72	(i) Single-crystal silicon (92.21% ^{28}Si; 4.70% ^{29}Si; 3.09% ^{30}Si; thick target). (ii) The total specific energy loss parametrized as $$(dE/d\varrho x) = (dE/d\varrho x)_n + (dE/d\varrho x)_e = -f(v),$$ where $f(v) = K_n(v_0/v) + K_e(v/v_0) - K_3(v/v_0)^3$ for $v \le v_c$, and $f(v) = A + B(v/v_0) + C(v/v_0)^2$ for $v \ge v_c$; $v_0 = c/137$ and ϱ is the density. The nuclear contribution, $(dE/d\varrho x)_n$, was considered to be important only at velocities $v < v_0$, with the parameter $K_n = 1.26K_n$(Bohr) where K_n(Bohr) is Bohr's estimate at $v = v_0$ [59]. K_n was assumed to have a 25% uncertainty. The electronic contribution, $(dE/d\varrho x)_e$, was calculated using the effective charge concept of Booth and Grant [60], to interpolate the available experimental data. For fixed K_n, parameter v_c was varied within $1.5 \le v_c/v_0 \le 10$ in order to fit the parameters to the interpolated stopping-power data, requiring continuity of the function $f(v)$ and of its derivative at $v = v_c$. The electronic stopping power was assumed to have a 5% uncertainty. The stopping power uncertainties were taken into account. Doppler-broadened line-shape analysis.
[33]	^{4}He(^{32}S,$\alpha'\gamma$) 5.45	(i) Copper implanted with ^{4}He (6×10^{17} atoms/cm^2). (ii) The effect of a 5% uncertainty in the experimental electronic stopping power from Ref. [69] was included. An analytic expression reproducing the LSS nuclear stopping power curve [51] along with Blaugrund's approximation [61] at low recoil velocities. Doppler-broadened line-shape analysis.
[40]	^{32}S(n,n') 0.32	(i) Thick sulfur targets bombarded with fast reactor neutrons. (ii) Uncertainty in the stopping power not included. $F(\tau)$ analysis.
[50]	^{28}Si(α,γ) 0.45	(i) Evaporated Si or $^{28}SiO_2$ (a few keV thick) on gold. Composition of the deposit mostly SiO. (ii) Details not given. $F(\tau)$ analysis.
[34]	^{4}He(^{32}S,$\alpha'\gamma$) 6.21	(i) Fe (2 mg/cm^2) implanted with ^{4}He on silver. (ii) Stopping powers were taken from the tabulation by Ziegler [62]. Stopping power uncertainty included. Doppler-broadened line-shape analysis.
[12]	^{29}Si$(\alpha,n\gamma)$ 1.37	(i) SiO_2 (88% ^{29}Si, 300μg/cm^2) on tantalum. (ii) As in Ref. [26] above. The electronic stopping powers taken from Ref. [63]. A 15% error added in quadrature to account for uncertainties of the stopping power. $F(\tau)$ analysis.
This work	^{2}H(^{31}P,n) 4.50	(i) Gold implanted with ^{20}Ne and ^{2}H (3.1×10^{16} atoms/cm^2 and 6.2×10^{17} atoms/cm^2, respectively). Silicon implanted with ^{2}H (6.2×10^{17} atoms/cm^2). (ii) Experimentally verified or semiempirical stopping powers as described in the text. Computer simulation of the slowing-down and experimental conditions. Uncertainty in the stopping power included. Doppler-broadened line-shape analysis.
This work	^{28}Si(^{6}Li,pn) 1.84	(i) Tantalum implanted with ^{28}Si (6.2×10^{17} atoms/cm^2). (ii) As in the previous item.

TABLE II. (*Continued*).

Ref.[a]	Reaction[b] v/c (%)	(i) Slowing-down medium. (ii) Stopping powers and DSA analysis.[c]
This work	^{31}P(p,γ) 0.21	(i) Tantalum implanted with ^{31}P (2.0×10^{17} atoms/cm^2). (ii) As in the previous item.

[a]Listed in chronological order.
[b]In our notation ^{32}S$(\alpha,\alpha'\gamma)$, for example, means measurements of γ rays in coincidence with alpha particles and ^{29}Si(α,n) means measurements of singles γ-ray spectra. The v/c values correspond to the initial velocities calculated from the reaction kinematics. Only maximum values are shown.
[c]The LSS stopping powers [51] with Blaugrund's approximation [61] for the large-angle scattering have been used, if not stated otherwise.

to the beam direction. The stainless-steel target holder was air-cooled. It was essential to keep the carbon buildup on the target surface and oxidization of the target to a minimum (especially in the case of ^{6}Li$^+$ bombardment) because the interfering ^{12}C+^{6}Li and ^{16}O+^{6}Li reactions possess high reaction cross sections. The heat generated by the bombarding ion beam and the good vacuum (better than 2 μPa) maintained in the target chamber kept the carbon deposition rate to a minimum in each experiment. Furthermore, it was checked such that the analyzed γ-ray peaks did not overlap with the peaks possibly produced in the ^{12}C+^{6}Li or ^{16}O +^{6}Li reactions. These additional checks were made with 12-MeV ^{6}Li ions incident on targets of tantalum implanted with 100-keV ^{12}C (10^{17} ions/cm^2) or tantalum oxidized to Ta_2O_5 (400 nm thick). The energies of the ^{31}P beam were well below the Coulomb barrier for the ^{12}C+^{31}P reactions.

C. Reaction ^{31}P$(p,\gamma)^{32}$S

The ^{31}P$(p,\gamma)^{32}$S reaction studies with a 1.0- to 1.6-MeV proton beam having a typical intensity of 7 μA were performed at the 5-MV Van de Graaff accelerator of the Institute of Nuclear Research in Debrecen, Hungary. The beam was collimated to a spot 5 mm in diameter on the target, which was set perpendicular to the direction of the beam. The target holder provided direct cooling of the target backing. The collected charge of the spectra varied between 80 and 200 mC in the DSA lifetime measurements and between 300 and 600 mC in the branching ratio measurements — depending on the resonance strength and the detector-target distance. γ rays were detected using a 25% efficient Ortec HPGe detector. The energy resolution of the spectrometer system was 2.20 keV at E_γ=1.46 MeV and 3.01 keV at E_γ=2.61 MeV. The detector was shielded from the laboratory background radiation by 6 cm of lead. The γ-ray spectra were stored in an 8192-channel memory with dispersions of 0.7–1.0 keV/channel.

The γ decay of the 1557- and 1583-keV proton resonances — most promising for a study of several lifetimes in one measurement — were studied using an escape suppression arrangement wherein the HPGe detector was surrounded with a conical BGO veto detector provided by the Groningen Cyclotron Laboratory. An escape suppression factor of 6 was achieved.

The intensities of γ-rays were derived from spectra recorded with the detector at 55° with respect to the beam axis. The 1057-, 1557-, and 1583-keV resonances [31] were selected for the lifetime measurements during which the γ-ray detector was set at 0° and 90° relative to the beam direction.

D. Analysis of line shapes

The mean lifetimes of the levels in ^{32}S produced in the different reactions were deduced from the analysis of Doppler-broadened γ-ray line shapes. This analysis is based on computer simulations by the Monte Carlo (MC) method, where different factors affecting the line shape are realistically taken into account. In many cases, and especially when the γ-ray peaks overlap, the line shape analysis gives more detailed and more reliable information than the $F(\tau)$ analysis based only on γ-ray peak centroid shifts. Selected portions of γ-ray spectra along with the simulated best-fit line shapes are shown in Fig. 2. The inferred lifetime values are collected in Table III.

In the case of high-energy transitions ($E_\gamma \geqslant 2.7$ MeV), contents of adjacent channels in the spectra were summed. Line shapes recorded at 0° were fitted for all three reactions, but the 90° data were also used in the case of the ^{31}P(p,γ) reaction. Data from measurements with the silicon- and gold-backed targets in the ^{2}H$(^{31}$P$,n\gamma)^{32}$S reaction were both used, except in the cases of the 4.282- and 5.549-MeV levels. Their quoted lifetime values are based only on analysis of the silicon data.

In general, the simulated line shape is a sum of the shapes corresponding to the direct prompt and delayed feedings of a state. The sum is weighted by the experimental fractions of the feedings. These fractions were obtained from the measured populations of the ^{32}S states (at different bombarding energies) and from the γ-ray branching ratios reported in the literature [10–12] and in the current ^{31}P(p,γ) experiment. Delayed feeding was significant only in the ^{31}P(p,γ) reaction.

To extract a reliable value for a short lifetime ($\tau<100$ fs) especially when the kinematic broadening of a corresponding γ-ray line shape is comparable to or larger than the detector resolution and the full Doppler shift, it is important to have a realistic description for the distribution of initial recoil velocities. In the case of the ^{2}H$(^{31}$P$,n\gamma)$ reaction, an iterative procedure, described in Ref. [65], was used. In this method, an initial velocity distribution and a level lifetime were determined by combining γ-ray line shape data measured with two stopping materials with differing stopping powers. The

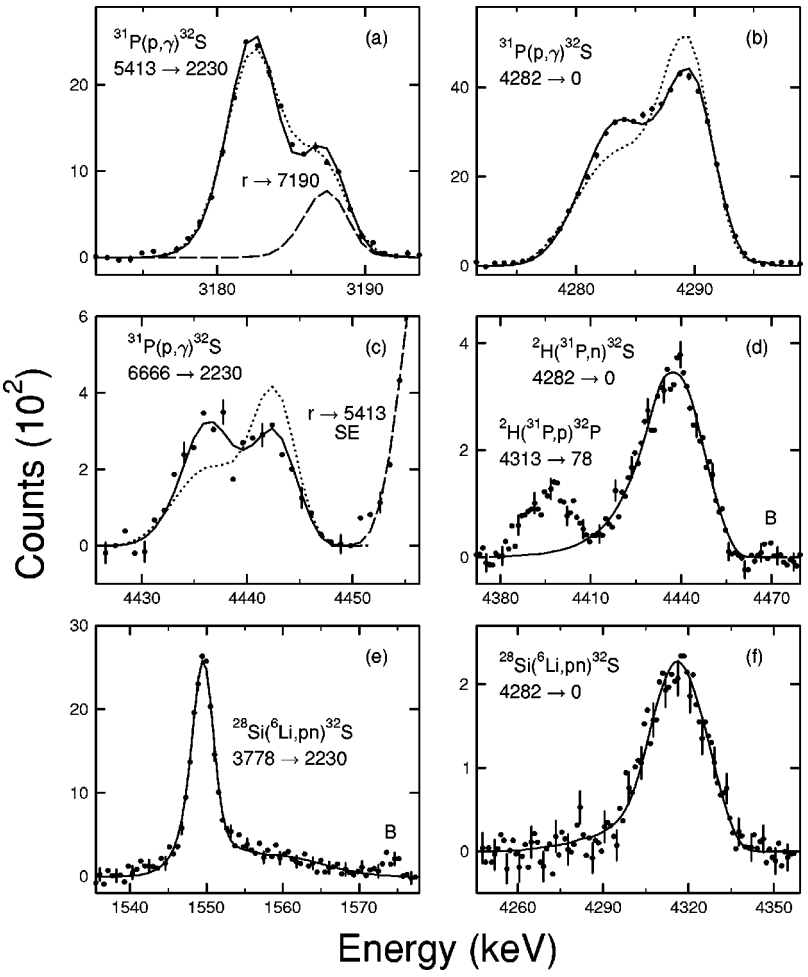

FIG. 2. Selected portions of background-corrected γ-ray spectra recorded in the ^{31}P$(p,\gamma)^{32}$S reaction measurements at the E_p=1557 keV resonance [(a)–(c)], in the ^{2}H(^{31}P,$n\gamma$)^{32}S reaction measurements at 24.6 MeV beam energy (d), and in the ^{28}Si(^{6}Li,$pn\gamma$)^{32}S reaction measurements at beam energies of 12.0 MeV (e) and 8.0 MeV (f). The γ-ray transitions are denoted in the figures (SE =single-escape peak, B=background peak). The solid lines illustrate the simulated best-fit line shapes corresponding to the lifetimes shown in Table III. In (a) the dashed line shows separately the contribution of the primary $r\rightarrow$7190 keV transition and in (c) the single-escape peak of the primary $r\rightarrow$5413 keV transition. For further details, see Sec. II F. The dotted lines in (a)–(c) correspond to the lifetime values of the levels adopted previously in the compilation of Ref. [11].

energy loss of the bombarding ^{31}P ion before the reaction was also taken into account in the determination of the initial recoil velocity. For each slowing-down simulation, the reaction depth was selected randomly within the implanted ^{2}H concentration distribution, the selection probability being proportional to the concentration of target atoms. The energy loss was calculated from the reaction depth using the stopping power values of Refs. [69] and [70] for ^{31}P in gold and in silicon, respectively.

When using the ^{6}Li projectiles, levels in ^{32}S can be produced via the competing ^{28}Si(^{6}Li,$pn\gamma$) and ^{28}Si(^{6}Li,$d\gamma$) reaction channels. At our incident energies, both reactions proceed primarily through the compound-nuclear channel [71]. This observation is supported by the large yield of the unnatural-parity 5.413-MeV, $J^{\pi}=3^{+}$ state in the current experiment. When the reaction is of the compound-nuclear type, it has also been shown [72] that the ^{28}Si(^{6}Li,$pn\gamma$) channel dominates over the ^{28}Si(^{6}Li,$d\gamma$) channel. In the MC simulations, the line shapes were assumed to be produced via the two competing contributions that were weighted with fractions calculated using the empirical model described in Ref. [72]. The initial velocity distribution was calculated by assuming an isotropic angular distribution in the center-of-mass frame for each emitted particle (proton and neutron or a deuteron). This approach was found to be sufficiently accurate such as to reproduce the experimental shapes in the simulations.

In the DSA analysis of (p,γ) data, it is usually assumed that the effect of the emission of the primary γ ray on the broadening of a secondary γ-ray peak can be neglected. This assumption can result, however, in a systematic error in the deduced lifetime as is reported in our recent study [6]. In the current analysis, the primary-γ-ray-induced broadening was included in the simulations.

Except for the slowing-down process described in the following, most other aspects of the MC simulation can be verified by analyzing the line shape of an extremely fast transition. These include, for example, the effects caused by the finite size of the γ-ray detector and the instrumental resolution. The ground-state transition from the 8.126-MeV level in ^{32}S (τ=0.230±0.035 fs, see Table I) provided a built-in cross-check of our analysis for the ^{2}H(^{31}P,$n\gamma$)^{32}S reaction. In the ^{31}P$(p,\gamma)^{32}$S reaction, fast primary transitions from the resonance states were used for these checks.

E. Stopping power

The stopping powers of the slowing-down media (silicon, gold, or tantalum) for ^{32}S ions were described in the line shape analysis according to the following equation:

TABLE III. Lifetimes of levels in ^{32}S obtained in the current work with the ^{2}H(^{31}P,$n\gamma$), ^{28}Si(^{6}Li,$pn\gamma$), and ^{31}P(p,γ) reactions. Lifetime values are corrected for delayed feedings and are based on line-shape analysis. In our notation 252 *40*≡252±40, 57.7 *20*≡57.7±2.0, etc.

	^{2}H(^{31}P,$n\gamma$)		^{28}Si(^{6}Li,$pn\gamma$)[a]	^{31}P(p,γ)[b]	
E_x (keV)	$E=24$ MeV τ(fs)	$E=29$ MeV τ(fs)	τ(fs)	τ(fs)	Adopted τ(fs)
2230				252 *40*	252 *40*
3778			1280 *130*	1300 *400*	1280 *130*
4282	60 *9*	60 *10*	57 *7*	57.7 *20*	57.8 *20*
4459					Not measured
4695				400 *40*	400 *40*
5006				380 *70*	380 *70*
5413			241 *35*	237 *40*	240 *35*
5549	84 *15*			95 *12*	91 *12*
5798	6.9 *30*	11.8 *30*			9.4 *30*
6224	99 *20*	112 *13*			108 *13*
6411			35 *5*		35 *5*
6581					Not measured
6621				800[c] *120*	800 *120*
6666				88 *8*	88 *8*
6762				375[c] *50*	375 *50*
6852					Not measured
7002	2.3 *12*	2.8 *12*		2.0[d] *7*	2.2 *7*
7115	7 *4*	3.6 *18*		2.3[d] *5*	2.5 *5*
7190	11 *4*	12 *3*			11.6 *30*
7350					Not measured
7434	10.0 *18*	11.7 *14*			11.1 *14*
7485	6.8 *20*	7.4 *17*		6.9 *17*	7.1 *17*
7536	6.3 *11*	3.3 *10*			4.7 *15*
7567					Not measured
7950				210[c] *50*	210 *50*

[a]Measurements done at 8.0 and 12.0 MeV beam energy.
[b]Most measurements were done at E_p=1557 keV.
[c]Measured at E_p=1583 keV.
[d]Measured at E_p=1057 keV.
[e]Up to 7.6 MeV, all known levels are listed; above 7.6 MeV we obtained a lifetime value only for the 7.950 MeV level.

$$\left(\frac{dE}{dx}\right)=\left(\frac{dE}{dx}\right)_e+\left(\frac{dE}{dx}\right)_n^{\mathrm{ZBL}}. \tag{1}$$

$$\left(\frac{dE}{dx}\right)_b=\frac{(\gamma Z)_a^2}{(\gamma Z)_b^2}\left(\frac{dE}{dx}\right)_a, \tag{2}$$

Experimental values of the electronic stopping power $(dE/dx)_e$ of gold for ^{32}S ions at velocities $v\geqslant 2.45v_0$ (Bohr velocity $v_0=c/137$, where c is the velocity of light) were taken from Ref. [69]. For lower velocities, the electronic stopping power was extended linearly to zero at $v=0$. An uncertainty of $\pm 4\%$ in the stopping power values was assumed. Because experimentally confirmed values are unavailable, the semiempirical electronic stopping power of silicon [70] was adopted, with an assigned $\pm 10\%$ uncertainty.

Experimental data on electronic stopping power of tantalum for ^{32}S ions at velocities relevant to the current analysis of the ^{28}Si(^{6}Li,$pn\gamma$) reaction data are also lacking. Therefore, semiempirical values from Ref. [70] were used. They were compared with the values obtained from the effective charge parametrization (Z_1 scaling):

where the numerical values of effective charges $(\gamma Z)_{a,b}$ were taken from Ref. [69]. The electronic stopping power values of tantalum for ^{32}S ions were deduced using this formula and the experimental data of Ref. [73] for ^{29}Si ions. At velocities $v=2v_0-4v_0$, the values were observed to differ from the semiempirical stopping powers by 3% at most. The correctness of the Z_1 scaling was further tested in the case of ^{32}S ions slowing down in gold. The experimental data for ^{29}Si ions in gold, taken from Ref. [73] and scaled to ^{32}S ions, were compared to experimental values of Ref. [69] and the semiempirical values [70]. Again the differences in the velocity region of $2v_0-4v_0$ were less than 4%, and no systematic variations between the three stopping powers were observed. Therefore, the semiempirical values with an assigned $\pm 9\%$ total uncertainty were used in the analysis. The quoted uncertainty includes the contributions of (i) a $\pm 6\%$ uncertainty of the experimental stopping data [73], (ii) an

TABLE IV. Gamma-ray decay of the E_p=1557- and 1583-keV resonances in the reaction $^{31}P(p,\gamma)^{32}S$. See also Sec. II F.

Final state E_x(keV)	J^π	1557 keV E_x=10.372 MeV $J^\pi=2^+;T=1$ Branching (%)	1583 keV E_x=10.398 MeV $J^\pi=4^-;T=1$ Branching (%)
0	0^+	0.30 *8*	
2230	2^+	7.6 *8*	0.20 *3*
3778	0^+		
4282	2^+	37.4 *26*	0.30 *19*
4459	4^+		1.00 *14*
4695	1^+	10.7 *10*	
5006	3^-	2.7 *3*	4.9 *6*
5413	3^+	12.6 *13*	0.10[b] *3*
5549	2^+	3.3 *4*	
5798	1^-		0.30[b] *6*
6224	2^-	2.5 *3*	<0.4[b]
6411	4^+		<0.4[b]
6581	0–4		
6621	4^-		82.0 *16*
6666	2^+	19.8 *18*	
6762	5^-		2.7 *4*
6852	4^+		1.60 *22*
7002	$1^+;T=1$	0.20 *7*	0.30[b] *7*
7115	$2^+;T=1$		
7190	1^+	1.5 *4*	
7350	3^+	(0.3)[a]	0.70[b] *11*
7434	1^-		
7485	2^+	1.40 *18*	
7536	$0^+;T=1$		
7567	5^+		0.30[b] *6*
7637	$0^+,1^+$		
7702	3^-		0.70 *9*
7883	4^+		
7885	$(0–2)^-$		
7921	$0^+,1^+$		
7950	4^-		4.7 *5*
7975	3^-		<0.4[b]
8126	$1^+;T=1$		0.20[b] *4*

[a]The primary transition could not be confirmed by secondary transitions (see Sec. II F).
[b]New transition.

assumed $\pm 5\%$ uncertainty of the scaling procedure, and (iii) the $\pm 4\%$ differences between the semiempirical values and the values based on the Z_1 scaling.

Although the velocities of the recoiling ^{32}S ions produced in the $^{31}P(p,\gamma)$ reaction at the current bombarding energies are so small ($v<0.3v_0$) that the nuclear stopping power dominates, the effect of the electronic stopping power cannot be neglected. Because experimental data on the electronic stopping power of tantalum for ^{32}S ions are not available at these low velocities, the semiempirical values from Ref. [70] were corrected by a factor obtained from analysis of experimental range data for chlorine ions in tantalum [74]. The MC simulation of the experimental stopping data with the inclusion of the polycrystalline structure of tantalum has resulted in a correction factor of $f_e=1.35\pm0.16$ for the semiempirical electronic stopping power in the case of ^{36}Cl ions slowing down in tantalum [74]. Because abrupt changes in the stopping power are not expected between adjacent atomic numbers, the same correction for ^{32}S ions in tantalum is used in the current analysis at low velocities. If the correction factor f_e were 1.0 instead of 1.35, the analysis would yield slightly longer lifetimes (for example 10, 51.5, and 540 fs instead of 10, 50, and 500 fs, respectively). Compared to the use of amorphous target structure in the simulations, the inclusion of the polycrystalline structure resulted in negligible change in the lifetime value, but the improved fit in the experimental line shape reduced its statistical uncertainty.

At moderate and high recoil velocities, as in the current experiment with the $^{28}Si(^6Li,pn\gamma)$ and $^2H(^{31}P,n\gamma)$ reactions, the inclusion of the crystalline structure of the slowing-down material in the simulations would make the simulations very time-consuming. In test simulations with the $^{28}Si(^6Li,pn\gamma)$ reaction, for a mean lifetime of about 400 fs, it was found that the corresponding line shape can be simulated equally well (less than 1% difference between amorphous vs polycrystalline background) and much faster by a code in which the slowing-down material is assumed to be amorphous. Therefore, the polycrystalline structure of the backing was taken into account only in the analysis of the low-velocity $^{31}P(p,\gamma)$ data.

The nuclear stopping power $(dE/dx)_n$ was calculated by the MC method, in which the scattering angles of the recoiling ions were derived directly from the classical scattering integral [75] and the interatomic interaction described by the universal Ziegler-Biersack-Littmark (ZBL) potential [70]. According to Ref. [73], the exact choice of potential is relatively unimportant when the recoil velocities are high, as in the case of the $^2H(^{31}P,n\gamma)$ and $^{28}Si(^6Li,pn\gamma)$ reactions. To account for possible effects of the uncertainty of the chosen potential, especially at low velocities produced in the (p,γ) capture reaction, a $\pm 6\%$ uncertainty was assigned for $(dE/dx)_n$. The uncertainties in electronic and nuclear stopping powers are reflected in the uncertainties quoted for the deduced lifetime values.

F. Results

1. Lifetimes

The lifetime results obtained in this work are summarized in Table III. Lifetimes obtained with different reactions used in the current work are in good mutual agreement in all cases. This fact supports our belief that (i) the current experimental conditions are well controlled in each case and (ii) the effects that are relevant at different velocities are described realistically in the line shape analysis. Our results are compared with previously reported values in Fig. 1 and Table I. As can be seen from Fig. 1 and Table I, lifetime results from the previous DSA measurements in ^{32}S show wide variations. In order to understand these variations further, the experimental conditions and analysis procedures of the DSA measurements are shown in Table II. To emphasize the superiority of the current results, some important points are discussed below.

The previous DSA experiments suffer mainly from the inconsistent target structures, stopping powers without ex-

perimental confirmation, and analysis methods prone to systematical errors. Targets consisting of relatively thick layers evaporated on metal backings limit the accuracy of short lifetimes ($\tau<100$ fs). The limitations emerge from: (i) the unknown composition of the evaporated layer (because of the use of compound materials, for example Zn_3P_2, SiO_2, and PbS), (ii) the reduced density of the target layer (up to 30%) from that of bulk material, and (iii) uncertain thickness and homogeneity of the target. In the current work, implanted targets with stable and well-known structure were used. The low recoil velocities and LSS stopping powers in combination with the Blaugrund approximation can cause systematical errors, which are not properly taken into account in the previous works. The error analysis of the stopping power is totally lacking in many cases, while some authors take an unfounded and large error value that is added quadratically to the statistical errors. In the current work, the uncertainties arising from the uncertainties in the nuclear and electronic stopping powers are realistically included in the MC simulations. The electronic stopping power was either experimentally known or semiempirical approximation verified by comparing with scaled stopping powers, and the nuclear stopping power was calculated from a realistic interatomic potential. From the previously reported 92 lifetime values, only 5 were deduced from line shape analysis, the remaining 87 are from $F(\tau)$ analysis. Reliable $F(\tau)$ analysis is possible only if γ-ray peaks are well separated; otherwise line shape analysis must be used. Most of the previous works utilize also only one type of nuclear reaction, while three different reactions with a total of 7 different bombarding energies were used here. An important source of error in some of the previous works is the failure to take into account the delayed feedings and detector geometry, all of which were taken into account in the current work.

Although reanalysis of the earlier DSA data might reduce the variations in the previous lifetime values, as we observed in the case of ^{32}P [65], for many instances there are not enough details on the experimental conditions available (see Table II) to enable any meaningful reanalysis.

Our lifetime value for the 2.230-MeV level (252 ± 40 fs), although not as accurate as in some studies, is in a good agreement with the weighted average (245 ± 11 fs) of the three most accurate Coulomb excitation results [23–25]. For some other levels, the current lifetime results disagree strongly with previous lifetime data. For example, in the case of the 5.413-MeV level, the previous (p,γ) measurements suggest a lifetime of $\sim$115 fs [31,36,43], while the (p,p') and (α,n) measurements suggest $\sim$195 fs [37,38]. The lifetime value adopted in Endt's compilation [11] is 150 ± 30 fs. The current ^{31}P(p,γ) measurement [see Fig. 2(a)] yields $\tau=237\pm40$ fs when the correction for the contaminating primary γ transition ($r\rightarrow7.19$ MeV) is taken into account while analyzing the line shape of the 5.413$\rightarrow$2.230-MeV transition. Without this correction, analysis of the current data would yield a lifetime value of about 150 fs. The longer lifetime value is supported by the result of 241 ± 35 fs obtained in the ^{28}Si(^{6}Li,$pn\gamma$) measurement.

Because of the large variations in the previous lifetime data and current improvements in the data analysis and experimental arrangements, the current lifetimes, when available, are suggested for the adopted lifetimes. For those levels whose lifetime was not obtained in the current work, we have adopted the weighted averages of the literature values. A notable exception is the 4.459-MeV level, for which a reliable lifetime value has been determined in an inverse-kinematics (high recoil velocity) $\alpha\gamma$-coincidence experiment by Simonis *et al.* [34]. We have adopted their value and rejected the values reported in Refs. [28,29,32,40,41] because the latter experiments had serious difficulties related to the overlapping γ rays from the 4.459$\rightarrow$2.230-MeV and 2.230$\rightarrow$0-MeV transitions.

2. Gamma-ray branchings

(a) Decays of the $E_p=1557$- and 1583-keV resonances. In this paper, we present the results obtained only from the $E_p=1557$- and 1583-keV resonances. The $E_p=1583$-keV resonance, by its γ decay, is strongly connected to the negative-parity bound states. Even though this decay has been measured several times [31,43,45], some discrepancies remain. The γ-ray branching ratios derived from the on-resonance 55° spectra are given in Table IV. The secondary decays of the 6.762-, 6.852-, 7.350-, and 7.950-MeV levels were also studied because their branchings differ strongly in previous works [31,43,45]. Some results from Table IV are discussed below.

$E_x=10.372$ MeV: Our branching ratios are in good agreement with earlier determinations [31,76] except for a new transition (0.2%) to the 7.002-MeV level and a possible transition (0.3%) to the 7.350-MeV level. The 7.350 $\rightarrow$4.695-MeV secondary transition, if present, could not be separated from the single-escape peak of the 5.413 $\rightarrow$2.230-MeV transition.

$E_x=10.398$ MeV: Altogether 18 primary transitions were identified from this resonance. For nine of these, our branching ratios are in reasonable agreement with previous determinations [31,76]. Six weak previously unreported primary transitions were identified (see Table IV). Two of these are $E3$ isoscalar transitions to the levels at 7.002 and 8.126 MeV, and the third is an $M3$ isovector transition to the level at 5.798 MeV. Three more transitions were observed to the levels at 5.413, 7.350, and 7.567 MeV. Only upper intensity limits are given for the three weak transitions to the levels at 6.224, 6.411, and 7.975 MeV. The 3.987- and 4.181-MeV peaks in our spectrum can represent either a primary transition to the 6.411-MeV level and a secondary transition to the 2.230-MeV level (a choice preferred by Vernotte *et al.* [43]) or a primary transition to the 6.224-MeV level and a secondary transition to the 2.230-MeV level. The placement of a primary transition to the 7.975-MeV level is uncertain because the secondary transitions from this level (given in Ref. [12]) were not observed.

(b) Decays of bound levels. The spectrum taken with good statistics at the $E_p=1583$-keV resonance provided branching ratios for several bound levels in ^{32}S. In general, the agreement with the values given in Table 32.13 of Ref. [10] was reasonable with the following exceptions.

$E_x=6.762$ MeV: This level decays $29\pm6\%$ to the 4.459-MeV level. In our γ-ray spectrum, the other strong 71%

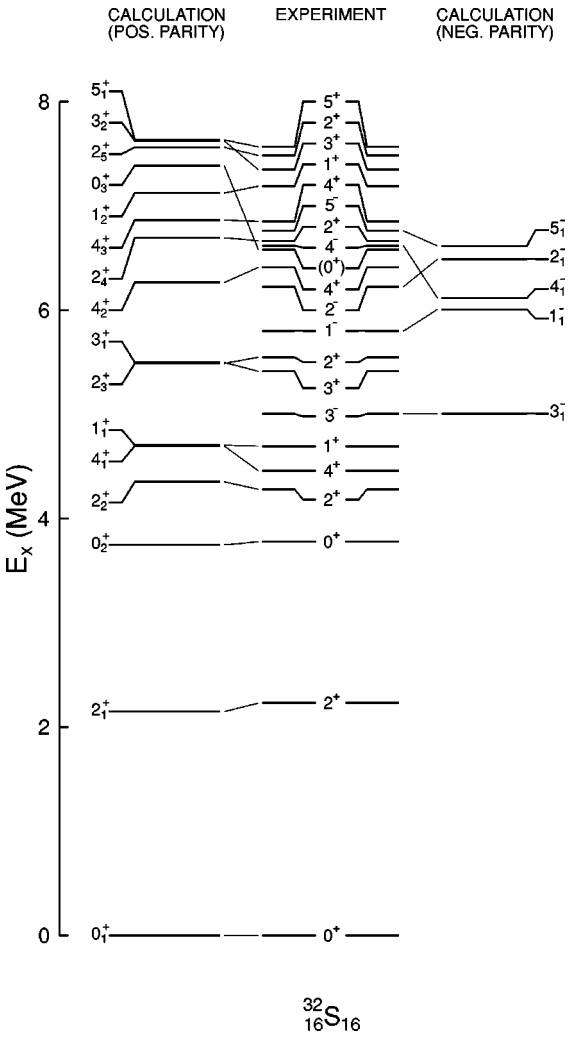

FIG. 3. Comparison of calculated and experimental level schemes for positive- and negative-parity $T=0$ states in ^{32}S. For the $T=1$ states and for additional $T=0$ states, see Sec. II F and Table VI. The calculated negative-parity spectrum is shifted down by 1160 keV so that the calculated and experimental energies of the first 3^- states match. Experimental energies and spin-parity assignments are from Ref. [12]. The uncertain assignment $J^\pi=0-4;\pi=$normal, given in Ref. [12] for the 6581-keV level, is here shown in parentheses as (0^+).

transition [10], 6.762→5.006 MeV, overlaps other transitions. No peak corresponding to the decay of 6.762→0 MeV is present in our spectrum, contrary to the report in Ref. [31].

E_x=6.852 MeV: This level decays to the 4.282- and 4.459-MeV levels with 73±7 and 27±4% branchings, respectively. This is in reasonable ageement with Ref. [10]. The 6.852→5.413-MeV transition previously reported in Refs. [77–79] was not observed. We give an upper limit of 2% for its intensity.

E_x=7.350 MeV: According to Refs. [12,77,78] this level decays 100% to the 4.695-MeV level. In our spectrum, the 7.350→4.695 MeV transition accounts for only 59±15% of the intensity of the primary transition. Therefore, the 7.350-MeV level may decay by other unknown branches as well.

E_x=7.950 MeV: The three observed transitions from this level to the 4.459-, 5.006-, and 5.413-MeV levels bear an intensity ratio 1:20:10. Brenneisen *et al.* [12] list only the transition to the 5.006-MeV level. These three transitions with intensities of 3±1%, 60±10%, and 30±10%, respectively, together account for 93% of the intensity of the primary transition. Taking into account the uncertainties in the γ-ray intensities, this imbalance is acceptable.

III. CALCULATIONS

A. Procedure

Shell-model calculations of excitation energies for both positive- and negative-parity states in ^{32}S and γ-decay properties for positive-parity states were performed using the shell-model program OXBASH [80]. The wave functions for all positive-parity states were obtained by constructing all possible configurations within the major oscillator shell defined by the $0d_{5/2}$, $0d_{3/2}$, and $1s_{1/2}$ orbitals (sd shell) and diagonalizing the effective Hamiltonian of Wildenthal [3]. The γ-decay properties for the positive-parity states were computed using harmonic oscillator radial wave functions with $\hbar\omega=(45A^{-1/3}-25A^{-2/3})$ MeV and effective $M1$ [81] and $E2$ [82] operators.

To account for negative-parity states, the model space must be extended beyond the sd shell to include $1\hbar\omega$ [one-particle, one-hole $(1p-1h)$] excitations into the next major shell — in particular, the $0f_{7/2}$, $0f_{5/2}$, $1p_{3/2}$, and $1p_{1/2}$ orbitals. The effective Hamiltonian was chosen to be the Warburton-Becker-Millener-Brown (WBMB) sd-fp shell Hamiltonian described in Ref. [83]. The WBMB Hamiltonian consists of the Wildenthal matrix elements for the sd shell, McGrory's fp-shell Hamiltonian for the fp-shell matrix elements [84], and a modification of the Millener-Kurath interaction for the cross-shell components [85]. Consequently, when no truncations are applied to the sd-fp model space, the $0\hbar\omega$ positive-parity states are the same as those in the sd-shell calculations described above.

In addition to the $sd\rightarrow fp$ shell excitations, negative-parity states can also arise from $1p-1h$ excitations of the closed ^{16}O core (i.e., the $0p_{3/2}$ and $0p_{1/2}$ orbitals) into the sd shell. However, because the $0d_{5/2}$ orbital is essentially filled, it is likely that excitations of this type will lie at a higher excitation energy than their $sd\rightarrow fp$ counterparts. This conjecture is supported in part by the fact that in the $T_z=\pm1/2$, $A=29-33$ nuclei, the lowest experimental negative-parity state has $J^\pi=7/2^-$ [86]. Hence, the excitation energies of the negative-parity states are based on calculations with only $1p-1h$, $sd\rightarrow fp$ excitations. In addition, it was found that because of computational difficulties, additional limitations on the configuration space were required. To keep the number of states with a definite angular momentum and isospin manageable, the model space was truncated so that no more than three holes in the $0d_{5/2}$ orbital were allowed. Also, as a result of difficulties encountered while projecting angular momentum with the shell-model program OXBASH, those configurations with three $0d_{5/2}$ holes and four $0d_{3/2}$ particles were excluded from the calculation. These limitations are based on the earlier shell-model study for ^{32}P [65], where it was noted that the overlap between the wave functions for the positive-parity states obtained with a similar truncation on the $0\hbar\omega$ space with those obtained from the

TABLE V. Experimental reduced $B(E1)$ transition probabilities in ^{32}S. The branching ratios and $M2/E1$ mixing ratios are from Ref. [11]. In our notation 115 *21*≡115±21 etc.

Initial state		Final state		$B(E1)$
E_x(keV)	J^π	E_x(keV)	J^π	(μW.u.)
5006[a]	3_1^-	2230	2_1^+	115 *21*
5798	1_1^-	0	0_1^+	530 *17*
6224	2_1^-	2230	2_1^+	140 *17*
6621[b]	4_1^-	4459	4_1^+	26 *5*
		5413	3_1^+	9.6 *20*
6762[c]	5_1^-	4459	4_1^+	61 *17*
7434	1_2^-	0	0_1^+	127 *36*
		2230	2_1^+	124 *64*
		3778	0_2^+	360 *190*
7950[d]	4_2^-	4459	4_1^+	3.2 *13*
		5413	3_1^+	85 *35*

[a] $B(E3;5.006\rightarrow 0)$=30 *7* W.u.

[b] $B(M2;6.621\rightarrow 2.230)$=0.08 *2* W.u.; $B(M2;6.621\rightarrow 4.459)$=0.09 *6* W.u.; $B(E2;6.621\rightarrow 5.006)$=11.7 *17* W.u. and $B(M1;6.621\rightarrow 5.006)$=0.21 *4* mW.u.

[c] $B(E2;6.762\rightarrow 5.006)$=15.3 *25* W.u.

[d] Branchings from the current (p,γ) experiment (see Sec. II F). $B(E2;7.950\rightarrow 5.006)$=1.7 *5* W.u. and $B(M1;7.950\rightarrow 5.006)$=0.035 *23* mW.u.

full sd-shell calculation was approximately 90%. Finally, the excitation energies for the negative-parity states were taken relative to $0\hbar\omega$ states obtained with the same model-space truncations. As in Ref. [65], the effect of the model-space truncations makes it difficult to predict the excitation energies of the negative-parity states relative to the positive-parity states with an accuracy much better than ~0.5 MeV.

At this point, the γ-decay properties of the lowest $T=0$, negative-parity states are difficult to describe theoretically with reasonable accuracy. First of all, after correcting for the recoil of the center of mass, the isoscalar $E1$ charge is identically zero [87]. In addition, negative-parity states may also decay via $M2$ transitions. Currently, little information is available regarding the effective $E1$ and $M2$ operators. Therefore, this work primarily focuses on electromagnetic transitions between the positive-parity, sd-shell states. In the future, when the computational restrictions imposed in this work are no longer necessary, a more comprehensive study of the decay properties of the negative-parity states may become feasible. Meanwhile, the experimental $B(E1)$ values are summarized in Table V.

B. Results

Shown in Fig. 3 and Table VI is a comparison between the experimental and theoretical spectra for both positive- and negative-parity states. With the exception of the level at 6.581 MeV, the experimental and calculated positive-parity states match almost perfectly up to the excitation energy of 7 MeV. The average deviation (absolute value) between theory and experiment is 85 keV and the root mean square (rms) deviation 261 keV (17 keV and 102 keV, respectively, if the 6581-MeV level is excluded). One-to-one correspondence between experimental and calculated levels can be further established up to 8.2 MeV and with slightly less confidence up to 9.1 MeV. At excitation energies above 7.0 MeV, $T=1$ states are also present, and for those states that can be identified with some confidence, the calculated excitation energies agree well with the experiment even up to 10 MeV. (See Ref. [65] for further discussion on the $T=1$ analog states in ^{32}P.) Despite the severe truncation applied in the calculations, a one-to-one correspondence for negative-parity states is found up to 8.2 MeV (and up to 9.1 MeV at a lower level of confidence). The calculated negative-parity $T=0$ states, shown in Fig. 3, have been shifted by −1160 keV relative to the positive-parity states (see Table VI for the unshifted energies) to match the energy of the lowest experimental $J^\pi=3^-$ state, which is the lowest negative-parity state. The chosen energy shift is almost equal to the energy shift needed to minimize the rms deviation between the experimental and calculated level energies.

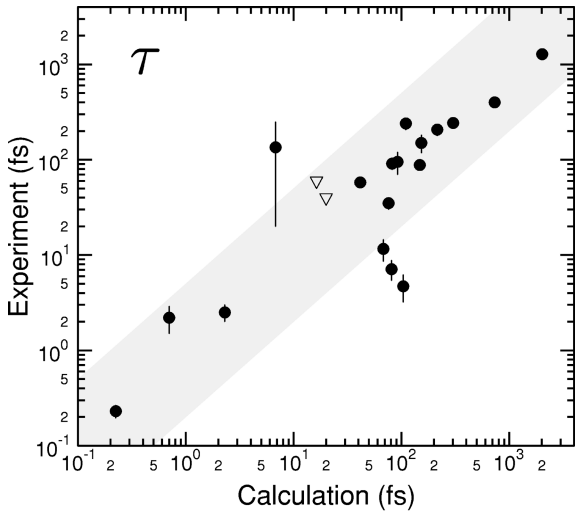

FIG. 4. Calculated mean lifetimes compared to those experimentally determined. Experimental upper limits are shown by open triangles. Calculated lifetimes agree with experiment to within a factor of 5 inside the shaded region.

To test the calculations further and to identify matches for those states that have no obvious counterpart in the predicted spectrum, electromagnetic decay properties were also examined. The branching and mixing ratios calculated from the theoretical $M1$- and $E2$-transition matrix elements are compared with the corresponding experimental values in Table VII. Because only a limited number of $E2/M1$ mixing ratios for positive-parity states and $M2/E1$ mixing ratios for negative-parity states are experimentally known, we have chosen also to compare the calculated lifetimes with experiment. This comparison is shown in Table VI and Fig. 4. Overall, the agreement is good. Indeed, only three cases ex-

TABLE VI. Comparison of experimental and calculated level energies and lifetimes in ^{32}S.

Experiment[a]			Calculation[b]			Experiment	Calculation[c]
E_x(keV)	J^π	T	E_x(keV)	J^π	T	τ(fs)	τ(fs)
0	0^+	0	0	0_1^+	0		
2230	2^+	0	2148	2_1^+	0	243 *11*	302
3778	0^+	0	3748	0_2^+	0	1280 *130*	2023
4282	2^+	0	4353	2_2^+	0	57.8 *20*	41.5
4459	4^+	0	4698	4_1^+	0	207 *29*	215
4695	1^+	0	4705	1_1^+	0	400 *40*	733
5006	3^-	0	6166	3_1^-	0	380 *70*	c
5413	3^+	0	5499	3_1^+	0	240 *35*	110
5549	2^+	0	5490	2_3^+	0	91 *12*	82
5798	1^-	0	7167	1_1^-	0	9.4 *30*	c
6224	2^-	0	7649	2_1^-	0	108 *13*	c
6411	4^+	0	6265	4_2^+	0	35 *5*	76
6581	0–4[d]	0	7388	0_3^+	0	e	135
6621	4^-	0	7277	4_1^-	0	800 *120*	c
6666	2^+	0	6695	2_4^+	0	88 *8*	148
6762	5^-	0	7778	5_1^-	0	375 *50*	c
6852	4^+	0	6866	4_3^+	0	95 *25*	92
7002	1^+	1	7058	1_1^+	1	2.2 *7*	0.7
7115	2^+	1	7052	2_1^+	1	2.5 *5*	2.3
7190	1^+	0	7125	1_2^+	0	11.6 *30*	68
7350	3^+	0	7626	3_2^+	0	e	128
7434	1^-	0	9328	1_2^-	0	11.1 *14*	c
7485	2^+	0	7563	2_5^+	0	7.1 *17*	81
7536	0^+	1	7312	0_1^+	1	4.7 *15*	104
7567	5^+	0	7634	5_1^+	0	150 *32*	153
7637	0^+,1^+	0	8019	0_4^+	0	e	60.5
7702	3^-	0	8688	3_2^-	0	e	c
7883	4^+	0	8131	4_4^+	0	e	109
7885	$(0–2)^-$	0	9157	2_2^-	0	e	c
7921	0^+,1^+	0	8691	0_5^+	0	e	65.2
7950	4^-	0	9435	4_2^-	0	210 *50*	c
7975	3^-	0	9111	3_3^-	0	<30	c
8126	1^+	1	8099	1_2^+	1	0.230 *35*	0.224
8191	4^+	0	8990	4_5^+	0	e	39.8
8270	$5^-(3^-)$	0	10207	5_2^-	0	<60	c
8281	3^+	0	8241	3_3^+	0	e	185
8296	3^-	0	9859	3_4^-	0	e	c
8344	2^+	1	8187	2_2^+	1	e	c
8346	$6^+(4^+)$	0	8854	6_1^+	0	<40	20.0
8380	2^- or $(1–3)^+$	0	9581	2_3^-	0	e	c
8407	2^+	0	8284	2_6^+	0	e	c
8492	1^-	0	10017	1_3^-	0	e	c
8507	0^+	0	9180	0_6^+	0	e	c
8690	2^+	0	8647	2_7^+	0	e	c
8729	3^+	1+0	8580	3_1^+	1	e	c
8746	3^+	0+1	9421	3_4^+	0	e	c
8861[f]	2^+	0	8922	2_8^+	0	e	c

TABLE VI. (*Continued*).

Experiment[a]			Calculation[b]			Experiment	Calculation[c]
E_x(keV)	J^π	T	E_x(keV)	J^π	T	τ(fs)	τ(fs)
9023	3^-	0	10332	3_5^-	0	[e]	[c]
9024	$6^-(4^-)$	0	9825	6_1^-	0	265[g] *55*	[c]
9060	$(1,2)^-$	0	10703	2_4^-	0	[e]	[c]
9065[h]	4^+	0	9427	4_6^+	0	88[i] *8*	77.2[j]
9235	2–5	0	8918	5_2^+	0	<60[g]	16.3
9783	$6^+(4^+)$	0	9636	6_2^+	0	135[g] $^{125}_{105}$	6.8

[a]The experimental energies and spin-parity and isospin assignments are from Refs. [11,12].
[b]In Fig. 3, the calculated negative-parity spectrum is shifted down by 1160 keV so that the energies of the first 3^- states match.
[c]Lifetimes are calculated only for positive-parity states in the cases where either the lifetime or the branching ratios are experimentally known.
[d]Natural-parity state.
[e]Lifetime not measured.
[f]Levels above 8864 keV are proton unbound.
[g]The given lifetime corresponds to the total width of the level.
[h]Below this energy, all known levels are listed.
[i]The given lifetime corresponds to a total radiative width Γ_γ=7.44 *67* meV [50].
[j]The inversion of the calculated 4_5^+ and 4_6^+ states would yield the lifetime value of τ=17 fs.

hibit a deviation between experiment and theory that is larger than a factor of 5.

In the cases where the mixing ratio is known experimentally or the transition is a pure multipole, we have in Table VIII compared the experimental $M1$ and $E2$ reduced transition probabilities with the calculated values. In the calculation of predicted lifetimes (see last column of Table VI), experimental energies were used. From these lifetimes and the calculated branching and mixing ratios given in Table VII, the individual transition strengths or matrix elements can be deduced as more experimental mixing ratios become available.

Referring to Table VI, the first experimental level missing an obvious corresponding model state is at 6.581 MeV. This level is excited strongly in (α,α') and is observed to decay only to the 2.230-MeV level [88]; therefore, $J^\pi=0^+$, 1^-, 2^+, 3^-, or 4^+. In the calculated spectrum of positive-parity states, the first predicted state without a corresponding experimental level is the third $J^\pi=0^+,T=0$ state at 7.388 MeV to which the 6.581-MeV level is identified here. The $J^\pi=0^+,T=0$ assignment is also favored in Ref. [92] on the basis of (p,p') angular distribution. On the other hand, Brenneisen *et al.* [12] assign negative parity to the 6.581-MeV level [leading to $J^\pi=1^-$ or 3^- when combined with the (α,α') results] on the basis of calculations using a weak (quadrupole-octupole phonon) coupling model. However, our calculated negative-parity spectrum does not easily allow association of the 6.581-MeV level to any negative-parity state below 8.5 MeV.

A systematic study of $J^\pi=0^+$ and 1^+ states (with possible T identification) in sd-shell nuclei was attempted by Crawley *et al.* [92] by measuring the angular distributions in high-energy (201-MeV) (p,p') reactions. In ^{32}S, these authors have identified five 1^+ states between 6.9 and 8.2 MeV. In our shell-model calculations, there are only three 1^+ states [at 7.058, 7.125, and 8.099 MeV (see Table VI)] that we have identified with the experimental levels at 7.002, 7.190, and 8.126 MeV, respectively. If the levels at 7.637 and 7.921 MeV indeed are $J^\pi=1^+$, $T=1$ states as suggested in Ref. [92], they have no theoretical counterparts. Moreover, these two levels would then correspond to excitations in ^{32}P at 0.634 and 0.918 MeV, respectively. Such levels have neither been observed nor predicted. Brenneisen *et al.* [12] have also noticed this discrepancy and have changed the J^π assignments of the 7.637- and 7.921-MeV levels from definite 1^+ to $J^\pi=0^+,1^+$. We favor this change. We then proceed to identify these levels with the theoretically calculated $0_4^+,T=0$ and $0_5^+,T=0$ states at 8.019 and 8.691 MeV, respectively (see Table VI) even though the energy agreement is poor.

As can be seen from Tables VI and VII, the calculated level energies, branching ratios, and lifetimes for the $J^\pi=5^+$ and 6^+ high-spin states in ^{32}S are in good agreement with experiment. This behavior is contrary to the common thinking that the high-spin, high-energy states suffer from mixing with the components outside the sd model space more than the low-spin states.

The experimental and predicted reduced transition probabilities are listed in Table VIII and illustrated in Fig. 5. They are in reasonable agreement. Only 4 out of the 21 reduced $E2$ transition probabilities compared herein are drastically underestimated, while all others are predicted to within a factor of 5. As in the case of ^{32}P [65], good agreement between theory and experiment (within a factor of 2) is achieved for the cases where the predicted reduced $E2$ transition probabilities are in the range $\sim$0.2$-$10 W.u. On the other hand, the smaller theoretical reduced $E2$ transition probabilities tend to underestimate the experimental data. Two out of the four discrepant $E2$ transitions are from the

TABLE VII. Comparison of experimental and calculated branching ratios and mixing ratios for positive-parity states in ^{32}S. Only those branchings that differ significantly from zero are given. All J^π assignments are from Refs. [11,12].

Initial state		Final state		Branching (%)		Mixing ratio $\delta(E2/M1)$[a]	
E_x(keV)	J^π	E_x(keV)	J^π	expt.[b]	calc.	expt.	calc.
2230	2^+	0	0^+	100	100		
3778	0^+	2230	2^+	100	100		
4282	2^+	0	0^+	85.9 *6*	90.1		
		2230	2^+	14.1 *6*	9.92	$+16\,^{25}_{6}$	−8.4
4459	4^+	2230	2^+	100	100		
4695	1^+	0	0^+	40 *1*	12.0		
		2230	2^+	60 *1*	88.0	+0.5 *2*	−0.63
5413	3^+	0	0^+	<1			
		2230	2^+	100	96.7	−7.5[c] *19*	−10.9
		3778	0^+	<4			
		4282	2^+	<3	2.64		−3.9
		4459	4^+	<1	0.70		−2.4
		4695	1^+	<1	<0.01		
		5006	3^-	<2			
5549	2^+	0	0^+	40 *1*	80.0		
		2230	2^+	60 *1*	17.7	−0.55[d] *20*	−4.8
		3778	0^+	<1	1.85		
		4282	2^+	<1	0.26		−0.71
		4459	4^+	<1	<0.01		
		4695	1^+	<1	0.21		−2.5
		5006	3^-	<0.4			
		5413	3^+	<5	<0.01		−0.01
6411	4^+	0	0^+	<4			
		2230	2^+	100	88.7		
		3778	0^+	<3			
		4282	2^+	<5	6.55		
		4459	4^+	<5	4.66		−4.8
		4695	1^+	<10			
		5006	3^-	<3			
		5413	3^+	<2	0.04		−2.7
6581	0–4^+	0	0^+	<3			
		2230	2^+	100[e]	43.3		
		4282	2^+		56.0		
6666	2^+	0	0^+	<3	21.1		
		2230	2^+	52 *4*	4.62		+1.9
		3778	0^+	48 *4*	62.6		
		4282	2^+	<7	1.95		+1.8
		4459	4^+	<3	2.80		
		4695	1^+		6.80		+2.1
		5006	3^-	<4			
		5413	3^+	<1	0.07		−0.17
6852	4^+	0	0^+	<7			
		2230	2^+	<7	44.1		
		3778	0^+	<8			
		4282	2^+	73 *6*	35.0		
		4459	4^+	17 *6*	18.4	$+0.93^{c,f}\,^{44}_{26}$	−3.7

TABLE VII. (*Continued*).

Initial state		Final state		Branching (%)		Mixing ratio $\delta(E2/M1)$[a]	
E_x(keV)	J^π	E_x(keV)	J^π	expt.[b]	calc.	expt.	calc.
		4695	1^+	<6			
		5006	3^-	<2			
		5413	3^+	10 *4*	2.46	−0.27[g] *7*	−3.5
7002	$1^+;T=1$	0	0^+	<1	25.2		
		2230	2^+	100	71.1		−0.006
		3778	0^+	<3	0.94		
		4282	2^+	<2	2.20		+0.003
		4459	4^+	<2			
		4695	1^+	<1	0.47		−0.09
		5006	3^-	<2			
		5413	3^+	<1	<0.01		
7115	$2^+;T=1$	0	0^+	3 *1*	6.23		
		2230	2^+	85 *2*	65.9	−0.381[h] *37*	+0.09
		3778	0^+	<1.4	0.03		
		4282	2^+	3 *1*	0.24		−0.13
		4459	4^+	<1	<0.01		
		4695	1^+	9 *1*	24.6		−0.010
		5006	3^-	<1			
		5413	3^+	<0.5	0.19		−0.051
		5549	2^+		2.77		+0.015
7190	1^+	0	0^+	40 *8*	29.8		
		2230	2^+	60 *8*	57.5		+5.3
		4282	2^+		2.73		+2.0
		4695	1^+		7.45		+12.0
		5549	2^+		1.85		+4.1
7350	3^+	2230	2^+		15.8		+0.77
		4282	2^+		2.61		+1.85
		4459	4^+		12.6		−0.31
		4695	1^+	100[i,j]	63.9		
		5549	2^+		3.89		+6.3
7485	2^+	0	0^+	100	19.9		
		2230	2^+		35.8		−9.2
		3778	0^+		21.7		
		4282	2^+		1.06		−36.4
		4459	4^+		2.27		
		4695	1^+		11.7		−18.5
		5413	3^+		2.53		+8.5
		5549	2^+		4.63		+3.0
7536	$0^+;T=1$	2230	2^+		72.6		
		4695	1^+	100	26.4		
		7190	1^+		0.97		
7567	5^+	4459	4^+	70[i] *10*	74.5	−9.7[c] $^{37}_{163}$	+12.5
		5413	3^+	30[i] *10*	22.9		
		6411	4^+		2.52		−8.0
7637	$0^+,1^+$	2230	2^+		85.9		
		4282	2^+	100[i]	0.003		
		4695	1^+		6.15		
		5549	2^+		5.53		
		7002	$1^+;T=1$		2.36		

TABLE VII. (*Continued*).

Initial state		Final state		Branching (%)		Mixing ratio $\delta(E2/M1)$[a]	
E_x(keV)	J^π	E_x(keV)	J^π	expt.[b]	calc.	expt.	calc.
7883	4^+	2230	2^+	75[i] *5*	12.3		
		4282	2^+		29.0		
		4459	4^+		17.1		−5.2
		5006	3^-	14[i] *5*			
		5413	3^+		7.06		−4.0
		5549	2^+	11[i] *5*	33.8		
7921	$0^+,1^+$	2230	2^+	100[i]	51.9		
		4282	2^+		41.4		
		4695	1^+		1.88		
		7002	$1^+;T=1$		4.34		
8126	$1^+;T=1$	0	0^+	87 *4*	78.3		
		2230	2^+	13 *4*	21.3		−0.06
8191	4^+	2230	2^+		82.8		
		4282	2^+	18[i] *3*	0.61		
		4459	4^+	28[i] *6*	6.14		+7.2
		5413	3^+	24[i] *5*	9.88		+9.9
		5549	2^+	30[i] *6*	0.09		
8346[k]	6^+	4459	4^+	>80[i]	99.0		
9065	4^+	2230	2^+	<1[l]	45.2		
		4282	2^+	12[l] *1*	34.5		
		4459	4^+	30[l] *3*	2.36	-11.4^{+63}_{-77}[m]	−2.59
		5413	3^+	58[l] *4*	0.23	+4.1[m] *6*	+0.36
		5549	2^+		11.4		
		6666	2^+		2.43		
9235[n]	5^+	4459	4^+	50[i] *5*	34.0		−42.6
		5413	3^+	50[i] *5*	54.5		
		6411	4^+		1.18		−4.7
		6852	4^+		10.1		−4.4
9783[k]	6^+	4459	4^+	100[i]	97.7		
		6852	4^+		0.99		
		7567	5^+		1.22		−4.8

[a]The sign convention of Rose and Brink [89] is used for the mixing ratios. Unless otherwise noted, the experimental values are from Refs. [10,11].
[b]Branchings are from Ref. [10], except where explicitly noted.
[c]The mixing ratio is from Ref. [12].
[d]The mixing ratio is from Poletti and Grace [90] who also give a value of $|\delta| > 6$.
[e]The branching is from Ref. [88].
[f]Ref. [12] gives also $|\delta| > 4$. Hentelä [91] gives $|\delta| < 9$.
[g]The mixing ratio is from Ref. [91].
[h]The mixing ratio is from Ref. [78].
[i]The branching is from Ref. [12]. In the case of the 7350-keV level, the branching is from Refs. [10,12].
[j]In the current work, this transition is observed to account for 59% of the intensity of the primary transition, the rest is unknown.
[k]Ref. [12] states also $J^\pi=4^+$ as a possible spin value.
[l]The branching is from Ref. [50].
[m]The mixing ratio is from Ref. [50].
[n]Ref. [12] states $J=2$–5 as possible spin values. The calculated values suppose $J^\pi=5^+$.

TABLE VIII. Comparison of experimental and calculated reduced $M1$ and $E2$ transition probabilities between positive-parity states in ^{32}S. The experimental values are based on data given in Tables VI and VII.

Initial state		Final state		$B(M1)$ (mW.u.)		$B(E2)$ (W.u.)	
E_x(keV)	J^π	E_x(keV)	J^π	expt.	calc.	expt.	calc.
2230	2_1^+	0	0_1^+			10.1 *5*	8.1
3778	0_2^+	2230	2_1^+			11.9 *12*	7.5
4282	2_2^+	0	0_1^+			1.38 *5*	2.0
		2230	2_1^+	$0.035\,^{54}_{30}$	0.12	8.9 *5*	8.8
4459	4_1^+	2230	2_1^+			11.9 *17*	11.4
4695	1_1^+	0	0_1^+	0.31 *3*	0.05		
		2230	2_1^+	2.5 *5*	1.8	0.44 *29*	0.5
5413	3_1^+	2230	2_1^+	0.07 *4*	0.07	1.7 *3*	3.6
5549	2_3^+	0	0_1^+			0.113 *15*	0.2
		2230	2_1^+	4.4[a] *9*	0.08	0.5[a] *3*	0.7
6411	4_2^+	2230	2_1^+			3.0 *4*	1.2
6666	2_4^+	3778	0_2^+			3.7 *5*	2.8
6852	4_3^+	4282	2_2^+			9.2 *26*	4.6
		4459	4_1^+	2.0[b] *12*	0.3	1.6[b] *9*	3.2
7115	$(2_1^+, T=1)$	0	0_1^+			0.09 *4*	0.20
		2230	2_1^+	81 *16*	78	2.1 *6*	0.12
7190	1_2^+	0	0_1^+	3.0 *10*	0.4		
7485	2_5^+	0	0_1^+			0.81 *19*	0.01
7536	$(0_1^+, T=1)$	4695	1_1^+	300 *100*	4		
7567	5_1^+	4459	4_1^+	<0.05	0.03	2.2 *6*	2.3
		5413	3_1^+			4.7 *18*	4.4
8126	$(1_2^+, T=1)$	0	0_1^+	220 *40*	207		
9065[c]	4_6^+	4282	2_2^+			0.074 *9*	0.24
		4459	4_1^+	$0.008\,^{46}_{5}$	0.013	0.22 *3*	0.0017
		5413	3_1^+	0.24 *7*	0.017	1.29 *15*	0.00072

[a]The mixing ratio $|\delta|>6$ would yield $B(M1)<0.15$ mW.u. and $B(E2)$=2.1 *3* W.u.
[b]The mixing ratio of $4<|\delta|<9$ would yield $B(M1)$=0.046 $^{70}_{22}$ mW.u., and $B(E2)$=3.2 *16* W.u.
[c]The inversion of the calculated 4_5^+ and 4_6^+ states would yield $B(M1;9.065\rightarrow4.459)$=0.018 mW.u., $B(M1;9.065\rightarrow5.413)$=0.037 mW.u., $B(E2;9.065\rightarrow4.282)$=0.023 W.u., $B(E2;9.065\rightarrow4.459)$=0.28 W.u., and $B(E2;9.065\rightarrow5.413)$=2.01 W.u.

9.065-MeV level (see next paragraph). The remaining two $E2$ transitions are from 2^+ states at about 7.5 MeV, and may suffer from mixing of intruder configurations as is suggested in the case of ^{28}Si [93]. In the case of the reduced $M1$ transition probabilities, the agreement between experiment and theory is not quite as good, although half of the transitions are reproduced to within a factor of 5. The remaining $M1$ transitions are systematically underestimated in the calculations which may indicate isospin mixing in the experimental wave functions. The overall agreement for the $M1$ transitions in ^{32}S is about the same as in the case of ^{32}P [65].

The comparison of the measured and calculated reduced $E2$ transition probabilities suggests that the 4_5^+ and 4_6^+ states, identified with the experimental states at 8.182 and 9.065 MeV, appear inverted in the predicted spectrum (see Table VIII). The inversion would bring the predictions for the two grossly underestimated $E2$ transitions from the 9.065-MeV state into an excellent agreement with experiment, while the accuracy of the predictions for other $M1$ and $E2$ transitions would remain roughly equal. The disagreement between the experimental and predicted branching and mixing ratios remains in the inversion. The experimental lifetime of the 9.065-MeV state does not, however, support the inversion (see Table VI). The lifetime value of the 8.182-MeV state is unknown.

Because of the success of the spherical shell model in reproducing the experimental data, we have not pursued the alternate description of ^{32}S levels in terms of the deformed Nilsson-Strutinski model. However, there is some evidence for the latter. The 2.230-, 3.778-, 4.282-, 5.006-, 5.413-, and 6.411-MeV levels are excited in the current experiment with ^{6}Li projectiles. Of these, the 3.778-, 4.282-, and 6.411-MeV levels belong to the proposed superdeformed band, predicted by the Nilsson-Strutinski calculations [9]. It has been observed that the direct alpha transfer (^{6}Li,$d\gamma$) reaction channel excites strongly levels of n-particle–four-hole (np-$4h$) character. For instance, $4p$-$4h$ states in the doubly magic ^{16}O and ^{40}Ca nuclei are strongly excited by direct alpha transfer [94,95]. The $4p$-$4h$ states have been interpreted as belonging to superdeformed bands (^{16}O) or deformed bands (^{40}Ca) [96]. In the case of ^{32}S, the observed strong transitions are interband and not intraband. Therefore the descrip-

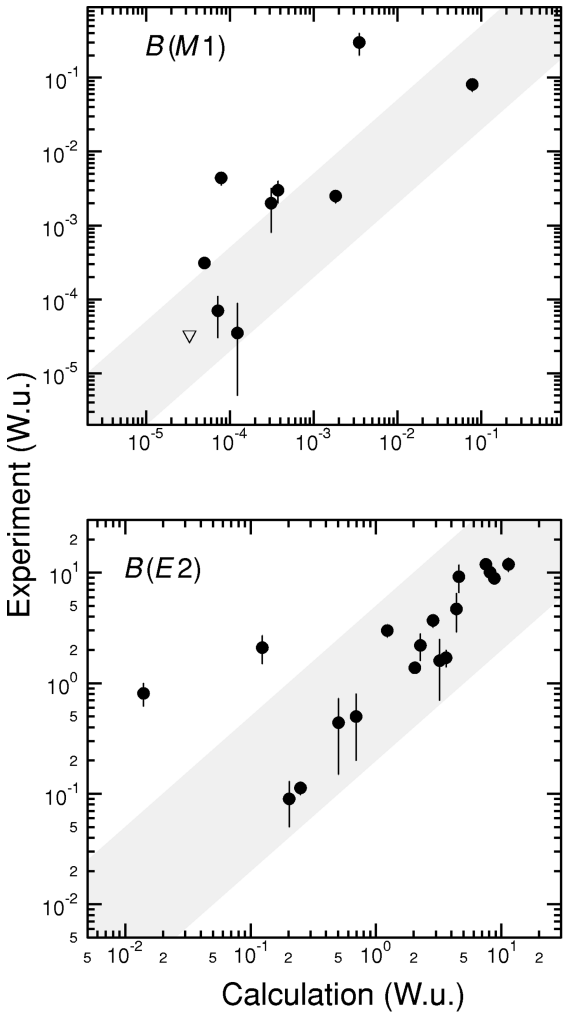

FIG. 5. Comparison of calculated and experimental reduced transition probabilities: $B(M1)$ (upper); $B(E2)$ (lower). Experimental upper limits are shown by open triangles. Calculated values agree with experiment to within a factor of 5 inside the shaded region.

tion of these states in terms of a superdeformed band cannot be strongly supported.

IV. SUMMARY

Lifetime values have been measured for 20 bound levels out of ~31 known levels below the excitation energy of 8.0 MeV in ^{32}S. The results based on reliable stopping powers in the DSA analysis and realistic MC simulations of the experimental conditions remove the large uncertainty of the lifetime values of excited ^{32}S levels reported in the literature. Shell-model calculations are able to reproduce the measured lifetimes to a reasonable degree. Also, the electromagnetic transition strengths are in most cases predicted correctly. A more detailed comparison requires additional information such as unambiguous J^π and T assignments and data on $E2/M1$ mixing ratios.

ACKNOWLEDGMENTS

The Groningen Cyclotron Laboratory is acknowledged for loaning the escape-suppression shield for the (p,γ) experiment. Gy. Güyrky is acknowledged for his help during the (p,γ) experiment. A. K. acknowledges support from the Magnus Ehrnroth Foundation. Zs. F., Á. Z. K., and E. S. acknowledge support from the Hungarian Science Foundation (OTKA) under Contract Nos. T016638 and CW015604. W. E. O. wishes to thank Oak Ridge National Laboratory for the use of computational facilities and acknowledges partial support from NSF Cooperative agreement No. EPS 9550481, NSF Grant No. 9603006, and DOE contract No. DE-FG02-96ER40985. The current research is supported by the Academy of Finland, the Hungarian Academy of Sciences, and the U.S. Department of Energy, the last-mentioned under Contract No. DE-AC05-96OR22464 with Lockheed Martin Energy Research Corporation (Oak Ridge).

[1] M. Carchidi, B. H. Wildenthal, and B. A. Brown, Phys. Rev. C **34**, 2280 (1986).
[2] B. Castel and I. S. Towner, *Modern Theories of Nuclear Moments* (Clarendon Press, Oxford, 1990), p. 200.
[3] B. H. Wildenthal, in *Progress in Particle and Nuclear Physics*, edited by D. H. Wilkinson (Pergamon, Oxford, 1984), Vol. 11, p. 5.
[4] I. Morrison, Phys. Lett. **91B**, 4 (1980).
[5] J. Keinonen, P. Tikkanen, A. Kuronen, Á. Z. Kiss, E. Somorjai, and B. H. Wildenthal, Nucl. Phys. **A493**, 124 (1989).
[6] P. Tikkanen, J. Keinonen, A. Kangasmäki, Zs. Fülöp, Á. Z. Kiss, and E. Somorjai, Phys. Rev. C **47**, 145 (1993).
[7] Y. T. Cheng, A. Goswami, M. J. Throop, and D. K. McDaniels, Phys. Rev. C **9**, 1192 (1974).
[8] P. Raghavan, At. Data Nucl. Data Tables **42**, 189 (1989).
[9] R. K. Sheline, P. C. Sood, and I. Ragnarsson, in *Capture Gamma-ray Spectroscopy* (Pacific Grove, CA, 1990), edited by R. Hoff, AIP Conf. Proc. **238** (AIP, New York, 1991), p. 533.
[10] P. M. Endt and C. van der Leun, Nucl. Phys. **A310**, 1 (1978).
[11] P. M. Endt, Nucl. Phys. **A521**, 1 (1990); **A529**, 763(E) (1991); **A564**, 609(E) (1993).
[12] J. Brenneisen, B. Erhardt, F. Glatz, Th. Kern, R. Ott, H. Röpke, J. Schmälzlin, P. Siedle, and B. H. Wildenthal, Z. Phys. A **357**, 157 (1997); **357**, 377 (1997).
[13] R. H. Helm, Phys. Rev. **104**, 1466 (1956).
[14] R. Lombard, P. Kossanyi-Demay, and G. R. Bishop, Nucl. Phys. **59**, 398 (1964).
[15] P. Strehl, Z. Phys. **234**, 416 (1970).
[16] E. C. Booth and K. A. Wright, Nucl. Phys. **35**, 472 (1962).

[17] E. C. Booth, B. Chasan, and K. A. Wright, Nucl. Phys. **57**, 403 (1964).
[18] D. L. Malaker, L. Schaller, and W. C. Miller, Bull. Am. Phys. Soc. **9**, 9 (1964).
[19] O. F. Afonin, A. P. Grinberg, I. K. Lemberg, and I. N. Chugunov, Yad. Fiz. **6**, 219 (1967) [Sov. J. Nucl. Phys. **6**, 160 (1968)].
[20] K. Nakai, J. L. Quebert, F. S. Stephens, and R. M. Diamond, Phys. Rev. Lett. **24**, 903 (1970).
[21] O. Häusser, T. K. Alexander, A. B. McDonald, and W. T. Diamond, Nucl. Phys. **A175**, 593 (1971).
[22] D. Schwalm, Thesis, Ruprecht-Karl-Universität Heidelberg, 1973.
[23] A. Olin, O. Häusser, T. K. Alexander, A. J. Ferguson, and W. Witthuhn, Nucl. Phys. **A221**, 555 (1974).
[24] D. Schwalm, E. K. Warburton, and J. W. Olness, Nucl. Phys. **A293**, 425 (1977).
[25] W. J. Vermeer, M. T. Esat, and R. H. Spear, Nucl. Phys. **A389**, 185 (1982).
[26] H. Grawe and K. P. Lieb, Nucl. Phys. **A127**, 13 (1969).
[27] J. P. Thibaud, M. M. Aleonard, D. Castera, P. Hubert, F. Leccia, and P. Mennrath, Nucl. Phys. **A135**, 281 (1969).
[28] G. T. Garvey, K. W. Jones, L. E. Carlson, D. A. Hutcheon, A. G. Robertson, and D. F. H. Start, Nucl. Phys. **A160**, 25 (1971).
[29] F. Ingebretsen, B. W. Sargent, A. J. Ferguson, J. R. Leslie, A. Henrikson, and J. H. Montague, Nucl. Phys. **A161**, 433 (1971).
[30] M. J. Renan and R. J. Keddy, Nuovo Cimento A **3**, 347 (1971).
[31] W. F. Coetzee, M. A. Meyer, and D. Reitmann, Nucl. Phys. **A185**, 644 (1972).
[32] Y. T. Cheng, A. Goswami, M. J. Throop, and D. K. McDaniels, Phys. Rev. C **9**, 1192 (1974).
[33] G. C. Ball, O. Häusser, T. K. Alexander, W. G. Davies, J. S. Foster, I. V. Mitchell, J. R. Beene, D. Horn, and W. McLatchie, Nucl. Phys. **A349**, 271 (1980).
[34] H. J. Simonis, F. Hagelberg, K. H. Speidel, M. Knopp, W. Karle, U. Kilgus, and J. Gerber, Z. Phys. A **330**, 361 (1988).
[35] S. Raman, C. H. Malarkey, W. T. Milner, C. W. Nestor, Jr., and P. H. Stelson, At. Data Nucl. Data Tables **36**, 1 (1987).
[36] C. J. Piluso, G. C. Salzman, and D. K. McDaniels, Phys. Rev. **181**, 1555 (1969).
[37] R. W. Ollerhead, T. K. Alexander, and O. Häusser, Can. J. Phys. **48**, 47 (1970).
[38] P. E. Carr, D. C. Bailey, L. L. Green, A. N. James, J. F. Sharpey-Schafer, and D. A. Viggars, J. Phys. A **6**, 705 (1973).
[39] A. Chevallier, E. Bozek, A. Pape, J. C. Sens, R. Armbruster, M. Langevin, and J. Vernotte, Nucl. Phys. **A176**, 401 (1971).
[40] D. Elenkov, D. Lefterov, and G. Toumbev, Nucl. Instrum. Methods Phys. Res. **201**, 377 (1982); Bulg. J. Phys. **10**, 498 (1983); Nucl. Instrum. Methods Phys. Res. A **228**, 62 (1984); M. K. Georgieva, D. V. Elenkov, D. P. Lefterov, and G. H. Toumbev, Fiz. Elem. Chastits At. Yadra **20**, 930 (1989) [Sov. J. Part. Nucl. **20**, 393 (1989)].
[41] G. T. Garvey, K. W. Jones, L. E. Carlson, A. G. Robertson, and D. F. H. Start, Phys. Lett. **29B**, 108 (1969).
[42] H. C. Evans, B. Castel, J. H. Montague, W. R. Paulson, and W. M. Zuk, Bull. Am. Phys. Soc. **13**, 87 (1968).
[43] J. Vernotte, J. M. Maison, A. Chevallier, A. Huck, C. Miehe, and G. Walter, Phys. Rev. C **13**, 984 (1976).
[44] P. R. Gardner, C. E. Moss, R. H. Spear, and L. E. Carlson, Aust. J. Phys. **25**, 659 (1972).
[45] H. Grawe, J. E. Cairns, M. W. Greene, and J. A. Kuehner, Can. J. Phys. **52**, 950 (1974).
[46] L. W. Fagg, W. L. Bendel, L. Cohen, E. C. Jones, Jr., H. F. Kaiser, and H. Uberall, Phys. Rev. C **4**, 2089 (1971).
[47] U. E. P. Berg, in *Proceedings of the International Conference on Nuclear Structure (contributed papers)* (Organizing Committee, Tokyo, 1977), p. 216.
[48] U. E. P. Berg, K. Ackermann, K. Bangert, C. Blasing, W. Naatz, R. Stock, K. Wienhard, M. K. Brussel, T. E. Chapuran, and B. H. Wildenthal, Phys. Lett. **140B**, 191 (1984).
[49] P. E. Burt, L. W. Fagg, H. Crannell, D. I. Sober, W. Stapor, J. T. O'Brien, J. W. Lightbody, X. K. Maruyama, R. A. Lindgren, and C. P. Sargent, Phys. Rev. C **29**, 713 (1984).
[50] J. D. MacArthur, S. P. Kwan, H. B. Mak, W. McLatchie, S. A. Page, S. S. Wang, and T. K. Alexander, Phys. Rev. C **32**, 314 (1985).
[51] J. Lindhard and M. Scharff, Mat. Fys. Medd. K. Dan. Vidensk. Selsk. **27**(15), 1 (1953); J. Lindhard, *ibid.* **28**(8), 1 (1954); J. Lindhard and M. Scharff, Phys. Rev. **124**, 128 (1961); J. Lindhard, M. Scharff, and H. E. Schiøtt, Mat. Fys. Medd. K. Dan. Vidensk. Selsk. **33**(14), 1 (1963).
[52] L. C. Northcliffe, Annu. Rev. Nucl. Sci. **13**, 67 (1963).
[53] J. H. Ormrod and H. E. Duckworth, Can. J. Phys. **41**, 1424 (1963).
[54] J. H. Ormrod, J. R. MacDonald, and H. E. Duckworth, Can. J. Phys. **43**, 275 (1965).
[55] J. R. MacDonald, D. F. H. Start, R. Anderson, A. G. Robertson, and M. A. Grace, Nucl. Phys. **A108**, 6 (1968).
[56] J. R. MacDonald, J. H. Ormrod, and H. E. Duckworth, Z. Naturforsch. A **21**, 130 (1966).
[57] E. F. Gibson, K. Battleson, and D. K. McDaniels, Phys. Rev. **172**, 1004 (1968).
[58] K. W. Dolan and D. K. McDaniels, Phys. Rev. **175**, 1446 (1968).
[59] N. Bohr, Mat. Fys. Medd. K. Dan. Vidensk. Selsk. **18**, 8 (1948).
[60] W. Booth and I. S. Grant, Nucl. Phys. **63**, 481 (1965).
[61] A. E. Blaugrund, Nucl. Phys. **88**, 501 (1966).
[62] J. F. Ziegler, *Handbook of Stopping Cross Sections for Energetic Ions in All Elements*, Vol. 5 (Pergamon, New York, 1980).
[63] L. C. Northcliffe and R. F. Schilling, Nucl. Data, Sect. A **7**, 233 (1970).
[64] Gy. Gyürky, Zs. Fülöp, Á. Z. Kiss, E. Somorjai, A. Kangasmäki, P. Tikkanen, and J. Keinonen, in *Proceedings of the Ninth International Symposium on Capture Gamma-ray Spectroscopy and Related Topics*, edited by G. Molnár, T. Belgya, and Zs. Révay (Springer-Verlag, Budapest, 1997).
[65] A. Kangasmäki, P. Tikkanen, J. Keinonen, W. E. Ormand, and S. Raman, Phys. Rev. C **55**, 1697 (1997).
[66] J. Jokinen, J. Keinonen, P. Tikkanen, A. Kuronen, T. Ahlgren, and K. Nordlund, Nucl. Instrum. Methods Phys. Res. B **119**, 533 (1996).
[67] J. Keinonen, J. Räisänen, and A. Anttila, Appl. Phys. A **34**, 49 (1984).
[68] A. Anttila, M. Bister, A. Luukkainen, Á. Z. Kiss, and E. Somorjai, Nucl. Phys. **A385**, 194 (1982).
[69] J. S. Forster, D. Ward, H. R. Andrews, G. C. Ball, G. J. Costa, W. G. Davies, and I. V. Mitchell, Nucl. Instrum. Methods **136**, 349 (1976).
[70] J. F. Ziegler, J. P. Biersack, and U. Littmark, in *The Stopping*

and Range of Ions in Solids, edited by J. F. Ziegler (Pergamon, New York, 1985), Vol. 1.
[71] M. Hugi, J. Lang, R. Müllerand, E. Ungricht, K. Bodek, L. Jarczyk, B. Kamys, A. Magiera, A. Strałkowski, and G. Willim, Nucl. Phys. **A368**, 173 (1981).
[72] A. C. Xenoulis, A. E. Aravantinos, C. J. Lister, J. W. Olness, and R. L. Kozub, Phys. Lett. **106B**, 461 (1981).
[73] K. Arstila, J. Keinonen, and P. Tikkanen, Nucl. Instrum. Methods Phys. Res. B **109**, 321 (1995).
[74] J. Keinonen, A. Kuronen, P. Tikkanen, H. G. Börner, J. Jolie, S. Ulbig, E. G. Kessler, R. M. Nieminen, M. J. Puska, and A. P. Seitsonen, Phys. Rev. Lett. **67**, 1 (1991).
[75] J. Keinonen, in *Capture Gamma-ray Spectroscopy and Related Topics*, Proceedings of the Fifth International Symposium on Capture Gamma-ray Spectroscopy and Related Topics, edited by S. Raman, AIP Conf. Proc. **125** (AIP, New York, 1985), p. 557.
[76] J. Vernotte, S. Gales, M. Langevin, and J. M. Maison, Nucl. Phys. **A212**, 493 (1973).
[77] I. Forsblom, P. Paukku, and S. Penttinen, Comments Phys. Math. **40**, 1 (1970).
[78] M. Viitasalo and I. Forsblom, Z. Phys. **269**, 173 (1974).
[79] C. E. Moss, R. H. Spear, F. Ahmad, A. M. Baxter, L. E. Carlson, and P. R. Gardner, Aust. J. Phys. **26**, 17 (1973).
[80] B. A. Brown, A. Etchegoyen, and W. D. M. Rae, computer code OXBASH, the Oxford-Buenos Aires-MSU shell model code, Michigan State University Cyclotron Laboratory Report No. 524, 1985 (unpublished).
[81] B. A. Brown and B. H. Wildenthal, Nucl. Phys. **A474**, 290 (1987).
[82] B. A. Brown and B. H. Wildenthal, Annu. Rev. Nucl. Part. Sci. **38**, 29 (1988).
[83] E. K. Warburton, J. A. Becker, and B. A. Brown, Phys. Rev. C **41**, 1147 (1990).
[84] J. B. McGrory, Phys. Rev. C **8**, 693 (1973).
[85] D. J. Millener and D. Kurath, Nucl. Phys. **A255**, 315 (1975).
[86] In ^{31}S and ^{33}Cl the assignment is uncertain, because $J^{\pi}=5/2^{-}$ is not excluded experimentally (see Ref. [11]).
[87] P. J. Brussaard and P. W. M. Glaudemans, *Shell-model Applications in Nuclear Spectroscopy* (North Holland, Amsterdam, 1977), p. 185.
[88] P. R. Gardner, D. C. Kean, R. H. Spear, A. M. Baxter, R. A. I. Bell, and L. E. Carlson, Aust. J. Phys. **26**, 747 (1973).
[89] H. J. Rose and D. M. Brink, Rev. Mod. Phys. **39**, 306 (1967).
[90] A. R. Poletti and M. A. Grace, Nucl. Phys. **78**, 319 (1966).
[91] R. Hentelä, Phys. Rev. C **23**, 1900 (1981).
[92] G. M. Crawley, C. Djalali, N. Marty, M. Morlet, A. Willis, N. Anantaraman, B. A. Brown, and A. Galonsky, Phys. Rev. C **39**, 311 (1989).
[93] P. M. Endt, J. G. L. Booten, Nucl. Phys. **A555**, 499 (1993).
[94] F. D. Becchetti, D. Overway, J. Jänecke, and W. W. Jacobs, Nucl. Phys. **A344**, 336 (1980).
[95] H. T. Fortune, M. N. I. Al-Jadir, R. R. Betts, J. N. Bishop, and R. Middleton, Phys. Rev. C **19**, 756 (1979).
[96] J. L. Wood, K. Heyde, W. Nazarewicz, M. Huse, and P. van Duppen, Phys. Rep. **215**, 101 (1992).